Food craving-like episodes during pregnancy are mediated by accumbal dopaminergic circuits

Roberta Haddad-Tóvolli, Sara Ramírez, Emma Muñoz-Moreno, Maria Milà-Guasch, Lluis Miquel-Rio, Macarena Pozo, Iñigo Chivite, Jordi Altirriba, Arnaud Obri, Alicia Gómez-Valadés, et al.

Food craving-like episodes during pregnancy are mediated by accumbal dopaminergic circuits

Roberta Haddad-Tóvolli[1,*], Sara Ramírez[1], Emma Muñoz-Moreno[2], Maria Milà-Guasch[1], Lluis Miquel-Rio[3,4,5], Macarena Pozo[1], Iñigo Chivite[1], Jordi Altirriba[6], Arnaud Obri[1], Alicia G Gómez-Valadés[1], Miriam Toledo[1], Elena Eyre[1], Analia Bortolozzi[3,4,5], Emmanuel Valjent[7], Guadalupe Soria[2,8,9], Marc Claret[1,10,11,12,*]

[1]Neuronal Control of Metabolism (NeuCoMe) Laboratory, Institut d'Investigacions Biomèdiques August Pi i Sunyer (IDIBAPS), Barcelona, Spain.

[2]Experimental 7T MRI Unit, Institut d'Investigacions Biomèdiques August Pi i Sunyer (IDIBAPS), Barcelona, Spain.

[3]Institut d'Investigacions Biomèdiques de Barcelona (IIBB), Consejo Superior de Investigaciones Científicas (CSIC), Barcelona, Spain.

[4]Institut d'Investigacions Biomèdiques August Pi i Sunyer (IDIBAPS), Barcelona, Spain.

[5]CIBER de Salud Mental (CIBERSAM), Madrid, Spain.

[6]Laboratory of Metabolism, Department of Internal Medicine Specialties, Faculty of Medicine, University of Geneva, Geneva, Switzerland.

[7]IGF, Univ. Montpellier, CNRS, INSERM, Montpellier, France.

[8]Laboratory of Surgical Neuroanatomy, Faculty of Medicine and Health Sciences, Institute of Neurosciences, Universitat de Barcelona, Barcelona, Spain.

[9]CIBER de Bioingeniera, Biomateriales y Nanomedicina (CIBER-BBN), Barcelona, Spain.

[10]CIBER de Diabetes y Enfermedades Metabólicas Asociadas (CIBERDEM), Barcelona, Spain.

[11]School of Medicine, Universitat de Barcelona, Barcelona, Spain.

[12]Lead contact

*__These authors jointly supervised this work:__ mclaret@clinic.cat; haddad@clinic.cat

Preparation for motherhood requires a myriad of physiological and behavioural adjustments throughout gestation in order to provide an adequate environment for proper embryonic development[1]. Cravings for high-palatable foods are highly prevalent during pregnancy[2] and contribute to the maintenance and development of gestational overweight or obesity[3]. However, the neurobiology underlying the distinct ingestive behaviours that result from craving specific foods remain unknown. Here we show that mice, similar to humans, experience gestational food craving-like episodes. These episodes are associated with a brain connectivity reorganization that affects key components of the dopaminergic mesolimbic circuitry, which drives motivated appetitive behaviors and facilitates the perception of rewarding stimuli. Pregnancy engages a dynamic modulation of dopaminergic signalling through neurons expressing dopaminergic receptors D2R in the Nucleus Accumbens, which directly modulate food craving-like events. Importantly, persistent maternal food craving-like behaviour has long-lasting effects on the offspring, particularly in males, leading to glucose intolerance, increased body weight, and increased susceptibility to develop eating disorders and anxiety-like behaviors during adulthood. Our results reveal the cognitively motivated nature of pregnancy food cravings and advocates for moderating emotional eating during gestation in order to prevent deterioration of the offspring's neuropsychological and metabolic health.

Pregnancy demands multiple physiological and behavioural adaptations to ensure a healthy embryonic development and preparation for maternal care[1]. Among them, metabolic and eating behaviour changes have been reported in diverse species[4–6]. A distinct example are food cravings, which are common features of human pregnancy, resulting in notable variations in maternal ingestive patterns towards consumption of high-palatable food (HPF)[2]. Problematically, recurrent food cravings contribute to the development and maintenance of gestational overweight/obesity[3],

with potential adverse health consequences for the offspring[7–9]. However, despite the widespread occurrence of gestational food cravings and having been documented for centuries[10], its underlying neurobiology remains unknown.

To verify the suitability of the mouse as a model to investigate pregnancy-characteristic food craving-like behaviour, we determined their drive to overconsume sweet-tasting items which are predominant cravings during human gestation[2]. We exposed C57BL/6 virgin and pregnant mice to a 2-bottle choice paradigm (Fig. 1a). To ensure a dynamic window of detectable preference changes, we identified the lowest sucralose and sucrose concentration that did not shift tastant selection in virgin females (Extended Data Fig. 1a, b, Fig. 1b, d). Remarkably, pregnant mice exhibited a higher inclination for both sweet compounds, suggesting increased sweetness sensitivity (Fig. 1b-e). Gestation did not disrupt the perception of the nutritional value of sugar since overall food intake was compensated (Extended Data Fig. 1c). To mimic human food cravings, we examined the motivation of pregnant mice to consume pleasant diet in a "limited access" paradigm[11] (Fig. 1f, Extended Data Fig. 1d). Pregnant females increased craving-like behaviour and daily food intake from the second week of pregnancy (Fig. 1g, Extended Data Fig. 1e). These results recapitulate the accentuated ingestion of palatable food observed during human gestation, thus validating the mouse as an appropriate model.

A prevalent hypothesis posits that gestational food-cravings are necessary to support embryonic growth[12]. To test this, we generated pseudopregnant females thus mimicking gestational features without actual embryonic development. Pseudopregnancy was validated by the presence of vaginal plugs and increased progesterone levels (Extended Data Fig. 1f). Pseudopregnant mice exhibited enhanced sweet sensitivity (Fig. 1b-e) and exacerbated compulsive eating similarly as genuinely-pregnant counterparts (Fig. 1g), without changes in daily food intake

(Extended Data Fig. 1e). These results suggest that pregnancy food craving-like behaviour does not arise to support embryonic growth.

Anxiety-like states can also promote compulsive eating[13]. Therefore, we questioned if gestation was associated with anxiety-like phenotypes that could alter eating patterns. Pregnant females showed unchanged exploratory time in the anxiety-related central area and total distance in the open field test, as well as equivalent performance in the dark-light box test when compared to virgin females (Extended Data Fig. 1g-j). Although not exhaustive, our results suggest that the distinct ingestive habits during gestation are not caused by major anxiety-related states.

Appetite and dietary patterns are controlled by a coordinated network of multiple and distributed neuronal circuits[14,15]. Thus, we reasoned that deviations in food consumption patterns during pregnancy may have a neural basis. To assess the female mouse brain resting-state architecture and uncover temporal features of the pregnant functional connectivity, we conducted functional Magnetic Resonance Imaging (fMRI) before, during and after pregnancy (Fig. 2a). The resting-state network was obtained by independent component analysis set to examine 20 independent components. Amongst them, 13 functional networks were identified[16] (Extended Data Fig. 2). Two of these networks (i.e., cortico-striatal and the salience networks) showed enhanced transient activity (based on amplitude analysis) during pregnancy (Fig. 2b-e). Spatial maps identified robust functional connectivity changes in gustatory, sensorimotor and reward centres during pregnancy (Fig. 2c, e). It is noteworthy that gestation was associated with changes in key components of the dopaminergic mesolimbic circuitry (dorsal and ventral striatum (Stri), ventral tegmental area (VTA), substantia nigra (SN)) that couple homeostatically-relevant stimuli with the incentive salience of palatable foods and motivated appetitive behaviours.

Based on our connectivity analysis, we explored whether gestation-associated functional mesolimbic system changes were associated with the remodelling of key molecular determinants

of dopamine circuits. Dopaminergic neurons in the VTA project and release this neurotransmitter into the ventral striatum, where it binds to its receptors (D1R and D2R) located mainly on medium-sized spiny neurons (MSNs). Tyrosine hydroxylase (*Th*; rate-limiting enzyme in dopamine synthesis) and dopamine transporter (*Slc6a3*) gene expression, as well as the number of VTA-TH^+/Fos^+ neurons and TH-producing neurons were unchanged in the VTA of pregnant mice (Extended Data Fig. 3a-d). *Drd1* and *Drd2* mRNA expression (encoding D1R and D2R respectively), as well as *Fos*-dependent activity, was unchanged in the dorsal striatum (dStri) during pregnancy (Extended Data Fig. 4a-e). However, in the nucleus accumbens (NAc; part of the ventral striatum), pregnant females displayed increased *Drd2* expression and augmented proportion of $Drd2^+/Fos^+$ neurons without changes in *Drd1* (Fig. 3a-d, Extended Data Fig. 4f). Enhanced accumbal *Drd2* expression returned to non-pregnant status after weaning of the offspring (Fig. 3c, Extended Data Fig. 4f). These results evidenced that gestation specifically upregulates NAc *Drd2* expression and activity of D2R neurons, suggesting that this receptor is the main dopaminergic effector involved in food craving-like behaviour.

Dopamine signalling via D2R engages two major intracellular pathways: the canonical $G_{\alpha i/o}$ protein-dependent and the non-canonical β-arrestin-dependent pathways[17]. While activation of the canonical route negatively regulates cAMP production, resulting in decreased PKA activity and subsequent inactivation of DARPP-32, the alternative pathway facilitates the activation (dephosphorylation) of Gsk3β through β-arrestin-2 and Akt (Fig. 3e)[17]. We examined whether pregnancy promoted molecular adjustments of these signalling routes. Dorsal striatal analysis revealed no changes in TH phosphorylation levels or markers for both downstream pathways (Extended Data Fig. 5a,b). In contrast, TH activity in the dopaminergic terminals that innervate the NAc was negatively modulated by gestation (decreased phosphorylation of TH-Ser40) (Fig. 3f, Extended Data Fig. 5c), likely compensating enhanced D2R signal transduction[18]. Furthermore,

129 the phosphorylation state of DARPP-32 and Gsk3β in the NAc of pregnant mice was attenuated
130 denoting engagement of both D2R-mediated dopaminergic signalling (Fig. 3g, Extended Data Fig.
131 5d). Collectively, these results suggest that pregnancy is associated with a dynamic modulation of
132 dopaminergic signalling mainly through accumbal D2R neurons at both pre-and postsynaptic
133 levels.

134 To gain deeper insights into the role of dopamine in food craving-like behaviour during
135 gestation, we measured this neurotransmitter and related metabolites. Dopamine content was
136 unaltered in the dStri, but it was increased in the NAc of pregnant mice (Fig. 3h, Extended Data
137 Fig. 5e). While the ratio between homovanillic acid (HVA) and dopamine was unchanged, the
138 relation between 3,4-Dihydroxyphenylacetic acid (DOPAC) and dopamine (a proxy of dopamine
139 turn-over) was decreased in both brain regions in pregnancy (Fig. 3i, Extended Data Fig. 5f). This
140 is likely the result of the augmented dopamine concentration in the NAc. Though its biological
141 meaning in the dStri is uncertain and presumably related with other pregnancy-related functions.

142 Decreased TH-Ser^{40} phosphorylation in the NAc probably reflects a mechanism to
143 counteract the increased dopamine content. This mechanism allows for faster adaptations to the
144 oscillatory nature of gestation and is less energy demanding than transcriptomic changes. Our
145 results have also shown an increase in *Drd2* expression concomitant with enhanced D2R signalling
146 in the NAc, suggesting a higher dopaminergic response (as a consequence of augmented dopamine
147 in this brain region) that may drive non-homeostatic feeding. These results support the idea that
148 the dopamine system is plastic and that particular physiological states modulate dopaminergic
149 connectivity and function.

150 We next explored dopamine signalling adaptations as causal determinants of gestational
151 food craving-like behaviour. To this end, we pharmacologically blocked dopaminergic
152 transmission in pregnant mice (Extended Data Fig. 6a). Notably, this approach suppressed

gestational food craving-like episodes, without affecting daily food intake or locomotor activity (Extended Data Fig. 6a-e). This suggests that dopaminergic receptor blockage restores the balance between D1R and D2R activity, preventing food-craving episodes. Our studies showed a specific activation of D2R-expressing neurons and remodelling of D2R-mediated signalling in the NAc during gestation (Fig. 3c, d, f, g, Extended Data Fig. 4f, 5c,d). Hence, we next aimed to define the involvement of D2R-expressing neurons in this brain region upon pregnancy-characteristic food craving-like episodes. To this purpose, we injected inhibitory (AAV-hM4Di) Designer-Receptors-Exclusively-Activated-by-Designer-Drugs (DREADDs) in the NAc (and dStri as control area) of pregnant *Drd2*$^{+/+}$ and *Drd2*$^{Cre/+}$ mice (Extended Data Fig. 7a-c). This permitted Cre-mediated silencing of D2R neuron activity upon Clozapine-N-oxide (CNO) injection[19,20], that in turn released their inhibitory tone on D1R-MSNs (Extended Data Fig. 7d-i). To exclude potential unspecific effects of CNO, both *Drd2*$^{+/+}$ and *Drd2*$^{Cre/+}$ mice were injected with this compound at a relatively low concentration that does not impact on behaviour[21]. Remarkably, this strategy normalized the exacerbated craving-like behaviour without changes in locomotor activity (Fig. 3j, Extended Data Fig. 7j-n). This effect was region-specific, as DREADD-mediated inhibition of D2R-expressing neurons in the dStri did not attenuate compulsive eating of pregnant mice (Fig. 3k, Extended Data Fig. 7o-s). CNO administration to *Drd2*$^{+/+}$ mice did not modify locomotor activity or general behaviour, as assessed by visual scrutiny. Altogether, these results demonstrate that gestation-related food craving-like behaviour is mediated by accumbal D2R-dependent circuits.

To examine the potential dichotomy of D2R canonical *vs.* non-canonical signalling underlying food craving-like behaviour, we injected the simultaneous D2R/β-arrestin partial agonist and D2R/$G_{\alpha i/o}$ antagonist UNC9994[22,23] to virgin and pregnant mice. UNC9994 administration to pregnant females blocked craving-like behaviour without changes in locomotor

activity (Extended Data Fig. 8a-f). Collectively, our chemogenetic and pharmacological studies suggest that gestational-specific craving-like episodes depends on the engagement of both canonical and non-canonical D2R pathways.

Maternal exposure to diverse dietary insults perturbs the development of neurocircuits implicated in psychological, appetitive and metabolic processes of the offspring[7–9]. Therefore, we questioned whether persistent food cravings during pregnancy affects the progeny's neuropsychological and metabolic status. To address this, we implemented the "limited access" protocol throughout gestation. To characterize the metabolic consequences of this paradigm on dams, and compare it with common maternal obesity protocols, we studied pregnant females exposed to either *ad libitum* chow diet, *ad libitum* Western diet (WD) or the "limited access" paradigm. WD-fed female mice showed a progressive body weight increase, glucose intolerance (in spite of unaltered fasted blood glucose and insulin levels) and higher plasma leptin (Extended Data Fig. 10a-e). These results indicate that the gestational "limited access" and maternal obesity protocols represent entirely different paradigms from the metabolic perspective.

Male and female offspring born to dams submitted to either continuous chow diet (chow-O) or "limited access" to HPF throughout gestation (HPF-O) were studied. At weaning (P21), HPF-O mice of both sexes were glucose intolerant when compared to chow-O counterparts without changes in body weight (Fig. 4a, b). Metabolic perturbations in HPF-O mice were accentuated in adulthood, particularly in male mice, that were heavier (Fig. 4c), exhibited increased adiposity (Fig. 4d) and persistent glucose intolerance (Fig. 4e). Next, we conducted a behavioural screening of anxiety-like phenotypes by testing the offspring to the open field, dark-light box and elevated plus maze paradigms. While individual tests showed some disparity (Fig. 4f-j, Extended Data Fig. 10a), the integration of these measures via z-normalization[24] showed more accentuated anxiety-like phenotypes in male HPF-O offspring (Fig. 4k). Maternal overnutrition and obesity have been

linked to cognitive dysfunction of the offspring[7,9]. Male HPF-O mice exhibited a trend to display cognitive impairments in the novel object recognition test (NORT) without changes in locomotion (Fig. 4l-n, Extended Data Fig. 10b). These results demonstrate that excessive food craving-like behaviour during gestation negatively impact offspring's neuropsychological and metabolic health.

Eating disorders often develop during adolescence[25]. To investigate the potential consequences of frequent food craving-like episodes during pregnancy upon progeny's disordered eating, we exposed adolescent (35 days old) Chow-O and HPF-O mice to a compulsive eating paradigm (Extended Data Fig. 10c). As expected[11], control animals did not escalate their caloric intake during the limited HPF access (Fig. 4o) but progressively increased total daily food consumption throughout the test (Extended Data Fig. 10d). In contrast, male HPF-O mice augmented their caloric intake during late compulsive eating episodes by ~35% more than at the start of the test (Fig. 4o). Compared with controls, male HPF-O animals exhibited higher basal daily food intake (chow-O: 8.48 ± 0.13 Kcal/day vs. HPF-O: 10.68 ± 0.26 Kcal/day, $p<0.01$; Extended Data Fig. 10d). The predisposition to compulsive eating was also observed in HPF-O females (Fig. 4o, Extended Data Fig. 10d). These findings evidenced that excessive maternal food craving-like behaviour confers offspring's susceptibility to develop eating disorders during adolescence.

Given that maternal high-fat diet feeding perturbs offspring dopamine signalling[26,27], we sought to determine whether recurrent gestational food craving-like events have a similar impact. Indeed, HPF-O mice of both sexes displayed a downregulation of both *Th* and *Slc6a3* expression in the VTA, with modest changes in the NAc and dStri (Extended Data Fig. 10e-j). Overall, the expression of dopaminergic system determinants was moderately attenuated in HPF-O, suggesting

that maternal compulsivity for HPF has long-term influences in hedonic gene expression and behaviour of the offspring.

The urgent appetitive behaviours during pregnancy suggest that cravings should be conceptualized as cognitively-motivated states[28]. Indeed, our results indicating that D2R-dependent circuits in the NAc mediate gestational food craving-like behaviour support this. The NAc acts as a hub integrating sensory, emotional and cognitive inputs into reward and motivated behaviours[29]. Enhanced D2R function promotes the incentive salience of food and emotional eating in mice and humans[30,31], and has been implicated in food addiction[32]. The augmented expression and activity of accumbal D2R neurons during pregnancy might reflect particular neurobiological adjustments associated with this physiological process, in which the connectivity from cortical regions into the NAc is remodelled. This may cause a vulnerability to cope with cognitively-motivated states, with subsequent intensification of food-craving episodes.

While our findings suggest that NAc-D2R neurons are key effectors of food craving-like behaviour during pregnancy, we cannot rule out the contribution of other brain areas with afferent projections into the NAc. For example, the enhanced connectivity observed in the medial prefrontal cortex (prelimbic and infralimbic cortices) and in the insula (part of the cortico-striatal and salience networks) during gestation could exert an interoceptive function, by integrating autonomic cues with emotional and motivational states[33]. Our results underline pregnancy as a physiological state able to promote plasticity of the neurocircuits connecting the prefrontal cortex and the basal ganglia. This could partially account for the conscious urge to food cravings, as described for prevalent addictions[34].

We show that recurrent gestational food craving-like behaviour compromises the metabolic and neuropsychological health of the progeny, enhancing the predisposition to eating and psychological disorders during adolescence and adulthood. These perturbations seem to

preferentially affect male offspring. Indeed, maternal obesity is generally associated with pronounced metabolic and cognitive impairments in male than in female offspring in both mice and humans[7-9]. The underlying causes of such sex dimorphism demand investigation. Additionally, the majority of programming studies to date have focused on long-term maternal insults, such as diet-induced obesity, undernutrition or permanent stress[7,9]. Our results indicate that even acute HPF consumption during food craving-like episodes is sufficient to originate detrimental health outcomes in the offspring thus advocating for controlled nutritional care during pregnancy.

Multiple theories have been proposed to explain the emergence of gestational food-cravings, including foetus nourishment, nutrient replenishment after nausea, hormonal fluctuations or cultural/psychosocial factors with inconclusive outcomes[2]. Our studies highlight biological and evolutionary-conserved attributes, that are independent of foetal growth demands, as the driving forces causing food craving-like experiences. Pregnancy entails a constant fluctuation of ovarian hormone levels. A concomitant increase in progesterone and oestrogen levels positively modulate food intake, as well as reward sensitivity and dopaminergic behavioural responses[35,36]. Therefore, it is tempting to speculate that variations in ovarian hormone levels during gestation contribute to food craving behaviours.

The purpose of food motivated behaviours during gestation remains elusive, but might have evolved to ensure the consumption of nutrient/caloric-dense food thus preventing energy deficits for periods of scarcity. In the modern lifestyle, this evolutive advantage has become detrimental and excessive food-cravings may affect mother and offspring health. In summary, our findings provide the cellular and mechanistic basis of pregnancy food cravings and evidence the benefits of moderating emotional eating during gestation.

Methods

Animal care, mouse lines and diets

Mice were maintained on a temperature controlled, 12-hour light/dark cycle with free access to water and standard chow (Teklad maintenance diet 14% protein; Envigo). For the "limited access" paradigm, Western diet (WD; 40% Kcal from fat and 43% Kcal from carbohydrates; Research Diets) was provided for 2 hours during 3 consecutive days a week[11]. C57BL/6 mice were bred in-house. *Drd2-Cre* mice have been previously described[37,38]. *Cre* negative littermates were used as controls. All animal studies were performed with approval of the Universitat de Barcelona Ethics Committee, complying with local government legislation (#10637).

Breeding strategy

C57BL/6, $Drd2^{+/+}$ or $Drd2^{Cre/+}$ female mice were mated at 9-12 weeks of age. Two females were housed with one male and vaginal plug was examined daily. Presence of plug denoted day 0.5 of gestation. Weight gain was measured weekly to confirm pregnancies. Dams were kept with their offspring until weaning. For pseudopregnant mice generation, eight-week-old C57BL/6 females were mated with vasectomized males. Presence of vaginal plug was considered positive pseudopregnancy.

Determination of sweet compound concentration

Eight-week-old C57BL/6 female mice were trained to drink from two water bottles until they reached a 50/50 preference. They were then presented to different concentrations of either sucralose (2.5; 1.0; 0.5; 0.1; 0.05 mM) or sucrose (200; 100; 50; 25 mM) and preference of each concentration against water was tested. The concentration at which virgin females were unable to

discern water from sweet compounds (50/50 intake) was determined and used in subsequent studies.

Two-bottle taste preference test

Eight-week-old C57BL/6 female mice fed with standard diet were individualized and trained to drink from two water bottles until 50/50 preference. They were then submitted to a two-bottle paradigm[39,40] to test preference for either sweet tastant (0.5 mM sucralose or 25 mM sucrose) or water during 3 experimental periods: i) before pregnancy; ii) throughout pregnancy with measurements every week; iii) one week after the weaning of the offspring (after pregnancy). Mice were overnight water deprived. At 09:00 a.m. two bottles containing sweet compound or water were provided. Mice were allowed to drink for 3 hours, without access to food. Total volume intake was measured and water was provided *ad libitum* until 7:00 p.m. Taste preference was calculated as the ratio between the sweet liquid consumption and the total volume ingested. Sweet preference and total food intake were measured daily. The position of the bottles was changed every day to exclude position effects. Control groups with virgin and a pseudopregnant females were run in parallel.

"Limited access" paradigm

The "limited access" paradigm was based on previous studies[11]. Briefly, eight-week-old C57BL/6, *Drd2*$^{+/+}$ or *Drd2*$^{Cre/+}$ female mice were individualized and habituated to WD during 5 days. After that, females had *ad libitum* access to chow and compulsive eating was induced by limited access to WD for 2 hours a day (at the end of the light cycle) during 3 consecutive days per week during 2 experimental periods: i) before pregnancy; ii) throughout pregnancy with measurements every week. Maternal food intake was measured daily. The percentage of daily caloric intake consumed

during the 2 hours of intermittent WD access was considered a proxy for food craving-like behaviour.

Maternal physiology measurements

For glucose tolerance test, E14.5-E16.5 pregnant females fed with chow diet (n=8), WD (n=8) or exposed to the "limited access" paradigm (n=8) were i.p. injected with D-glucose (2 g/kg) after 6 hours fasting. Blood glucose levels were measured using a glucometer (Nova Pro Biomedical). Plasma insulin and leptin levels were measured after fasting (6 hours) with commercial ELISA kits (Crystal Chem). Body weight was measured weekly.

Progesterone serum levels

Plasma samples were collected from C57BL/6 female mice at 3 different time-points: i) before pregnancy; ii) throughout pregnancy with measurements every week; iii) one week after the weaning of the offspring (after pregnancy). Control groups with virgin or pseudopregnant females were run in parallel. Levels of progesterone were determined using commercial kits (Crystal Chem).

MRI acquisition, processing and analysis

Each mouse was scanned at three time-points: i) before pregnancy (n=7); ii) during the second week of pregnancy (n=8); iii) one week after the weaning of the offspring (after pregnancy) (n=6). Experiments were conducted on a 7.0T BioSpec 70/30 horizontal animal scanner (Bruker BioSpin, Ettlingen, Germany), equipped with an actively shielded gradient system (400 mT/m, 12 cm inner diameter). The receiver coil is a surface coil for the mouse brain. Animals were sedated (4% isofluorane in 30% O_2 and 70% N_2), placed in supine position in a Plexiglas holder with a nose

cone for administering anaesthetic gases and fixed using tooth and ear bars. Eyes were protected from dryness with Siccafluid ophthalmologic fluid. Once placed in the holder with constant isoflurane (1.5%), a subcutaneous bolus of medetomidine (Domtor®, Orion Pharma) (0.3 mg/kg) was injected. For the next 15 minutes, the percentage of isofluorane was progressively decreased to 0.5%. Then, a continuous perfusion of 0.6 mg/kg/h of medetomidine was started and maintained until the end of the acquisition session. After completion of the imaging session, 1µl/g of atipamezol (Antisedan®, Orion Pharma) and saline were injected to reverse the sedative effect and compensate fluid loss. Localizer scans were used to ensure accurate position of the head at the isocenter of the magnet. Anatomical T2 RARE images were acquired in coronal orientation with effective TE=33ms TR=2.3s, RARE factor=8, voxel size=0.08x0.08 mm^2 and slice thickness=0.7 mm. rs-fMRI was acquired with an EPI sequence with TR=2s, TE=19.4, voxel size 0.21x0.21 mm^2 and slice thickness 0.5mm. 420 volumes were acquired resulting in an acquisition time of 14 minutes.

The rs-fMRI acquisition was processed to extract functional brain networks by independent component analysis (ICA) and evaluate differences in connectivity between pregnant and non-pregnant periods. Each fMRI acquisition was pre-processed including slice timing, motion correction, pass-band frequency filtering, spatial normalization to a mice brain atlas template and smoothing (ANTs and Python 3). All the pre-processed images were considered to extract the group ICA using FSL MELODIC. The resulting independent components were compared with the functional networks described[16] to identify the components corresponding to functional networks of interest. Afterwards, dual regression was performed to identify the network components and their spatial distribution in each individual brain and estimate the network shape and amplitude differences[41]. Network amplitude was defined as the standard variation of the time-series corresponding to the independent component (IC), and shape differences were analysed based on

the mean value of the z-score of the subject IC within the spatial map of the component (threshold at z=2.3). Kruskal-Wallis test was applied to identify differences between shape and amplitude values in the pregnant period vs. non-pregnant period in the selected ICs.

Quantitative polymerase chain reaction (qPCR)

VTA, dStri and NAc samples were dissected, immediately frozen in liquid nitrogen and stored at -80°C. Tissues were homogenized and total mRNA was isolated using Trizol (Invitrogen). Retrotranscription was performed using reagents from Applied Biosystems. Quantitative PCR was conducted using Premix Ex Taq mastermix (Takara) in an ABI Prism 7900 HT system (Applied Biosystems). TaqMan Gene Expression FAM/TAMRA probes (Applied Biosystems) used were: *Th* (Mm00447557_m1), *Slc6a3* (Mm00438388_m1), *Drd1* (Mm01353211_m1), *Drd2* (Mm00438545_m1). Gene expression levels were expressed relative to *Gapdh* (Mm99999915_g1).

Fluorescent in situ hybridization

Virgin, pregnant (during the second week of pregnancy) and after pregnancy C57BL/6 female mice were transcardially perfused with 4% paraformaldehyde (PFA). Dissected brains were post-fixed in 4% PFA at 4°C for 24 hours and cryoprotected. Brains were cut at 20µm on a cryostat and collected into 4 series (one every 4 sections) in SuperFrost Plus Gold slides (ThermoFisher) and subsequently stored at -80°C.

Fluorescent in situ hybridization for the simultaneous detection of *Drd1*, *Drd2* and *Fos* mRNA was performed using RNAscope. All reagents were purchased from Advanced Cell Diagnostics (ACD). All incubation steps were performed using the ACD HybEz hybridization system.

On assay day, one section series cut throughout the dStri and NAc was selected. From each animal, one section was incubated with the negative control probe to enable calculation of background. Slides were washed in PBS, baked at 60°C for 30 minutes and post-fixed with 4% PFA for 15 minutes. Sections were then dehydrated and baked for an additional 30 min at 60°C and submerged into boiling Target Retrieval reagent for 5 minutes. The slides were dehydrated in 100% ethanol, allowed to air dry for 5 minutes and placed into an RNAscope holder. Sections were treated with Protease III for 30 minutes at 40°C. Probe hybridization, amplification and detection, were performed according to the manufacturer's protocol. The colour module chosen labelled the *Fos* probe with Atto 550, the *Drd1* probe with Atto 647, and the *Drd2* probe with Atto 488. Sections were counterstained with DAPI and coverslipped with ProLong Gold Antifade Mountant (ThermoFisher) and stored in the dark at 4°C.

Images were taken using a confocal Leica DM 2500 microscope, equipped with a 40x/1.15 oil objective and using a zoom of 2x. Z-stacks of 1 µm of either the dStri or the NAc were captured bilaterally from 4 rostral to caudal sections per animal (n=3 animals/group). Laser intensities were kept constant throughout the entire image acquisition process. Images were imported into Fiji (NIH) where maximum intensity projections were made. To acquire the minimum intensity value for analysing the expression of *Drd1* and *Drd2*, the threshold for probe recognition was calculated as the mean cell intensity present in the negative control sections +3xSD. All labelling above this value was considered to be true signal[42]. Brightness and threshold were adjusted in all images. For quantification, 8-10 *Drd1*+ or *Drd2*+ neurons per section were manually selected and *Drd1* and *Drd2* particles were counted. After quantification, the presence of *Fos* expression was determined.

Western Blot

411 DStri and NAc were dissected and immediately frozen in liquid nitrogen and stored at -80°C. DStri
412 and NAc samples were sonicated in 120µl or 70µl, respectively, of RIPA buffer supplemented
413 with phosphatase and protease inhibitor cocktail (Sigma-Aldrich). Protein was quantified using
414 the BCA Protein Assay Kit (Pierce). 20µg for each sample and brain region were loaded onto a 4-
415 12% SDS–polyacrylamide gel (SDS-PAGE) (Bio- Rad). Proteins were separated by SDS-PAGE,
416 electrotransferred to PVDF membranes (Millipore), blocked in 5% BSA buffer and immunoblotted
417 overnight at 4°C with the following primary antibodies: mouse anti-tubulin (1:1000, Sigma), rabbit
418 anti-phospho-DARPP-32Thr34 (1:1000, Cell Signaling Technology), rabbit anti-phospho-
419 ThSer31 (1:1000, Millipore), rabbit anti-phospho-ThSer40 (1:1000, Cell Signaling Technology)
420 and rabbit anti-phospho-Gsk3βS9 (1:1000, Cell Signaling Technology). Membranes were
421 incubated for 1 hour at room temperature with secondary antibodies: anti-mouse IgG (1:5000, GE
422 Healthcare) or anti-rabbit IgG (1:5000, GE Healthcare). Detection was performed by enhanced
423 chemiluminescence (Pierce) and images were obtained using a LAS4000 (GE Healthcare). Protein
424 expression was quantified by densitometry using ImageJ software (NIH).
425
426 **Double Th and Fos immunofluorescence**
427 Selected 20 µm-thick sections (1 out of 4 sections) throughout the VTA (bregma between -3.10mm
428 and -3.70mm) of virgin, pregnant (during the second week of pregnancy) or after pregnancy
429 C57BL/6 female mice (n=3/group) were blocked with 2% chicken serum in PBS + 0.1% Triton
430 X-100 + 3% BSA and incubated with rabbit anti-Fos antibody (1:500; Synaptic Systems) in
431 blocking solution overnight at 4°C. As secondary antibody, a chicken anti-rabbit Alexa Fluor 488
432 (1:300; Life Technologies) in PBS + 0.1% Triton X-100 + 3% BSA was used. After washing,
433 slices were blocked with 2% donkey serum in PBS + 0.1% Triton X-100 and incubated with sheep
434 anti-Th antibody (1:600; Sigma) overnight at 4°C. As secondary antibody, a donkey anti-sheep

435 Alexa Fluor 594 (1:300; Life Technologies) in PBS + 0.1% Triton X-100 was used. For
436 quantification, representative images throughout the VTA of each animal were acquired using a
437 Leica DMI 6000B confocal microscope equipped with a 20x objective. The total number TH+
438 neurons and the proportion of TH+/Fos+ was counted manually using FIJI (ImageJ) software.
439
440 **Neurochemical analysis**
441 DStri and NAc samples of virgin (n=9) and pregnant (n=8) mice were dissected on a cold plate,
442 weighted, immediately frozen in liquid nitrogen and stored at -80°C. Dopamine, DOPAC and
443 HVA content were determined by HPLC with electrochemical detection (Waters model 2465,
444 +0.75 V) as described[43]. Tissues were homogenized in 200 µl (dStri) or 40 µl (NAc), respectively,
445 of buffer containing 0.4 M perchloric acid with 0.1% sodium metabisulphite, 0.01% EDTA, 0.1%
446 cysteine and centrifuged at 12,000g for 30 minutes. Aliquots of supernatants were filtered through
447 0.45 µm pore size filters (Millex) and analyzed by HPLC as described. The mobile phase consisted
448 of 0.1 M KH_2PO_4, 1 mM octyl sodium sulphate, 0.1 mM EDTA (pH 2.65) and 18% methanol.
449 Dopamine and their metabolites were separated on a Kinetex Core-Shell columns (C18, 2.6 µm,
450 75 × 4.6 mm; Phenomenex).
451
452 **Pharmacological blockage of dopamine receptors**
453 Eight-week-old C57BL/6 female mice were i.p. injected with the D1R/D2R dopamine receptor
454 antagonist cis-(Z)-Flupenthixol dihydrochloride (flupenthixol, 0.4 mg/kg; Sigma) or saline
455 (vehicle) and exposed to the "limited access" paradigm or open field test 30 minutes later. The
456 drug was prepared 5 minutes before the tests.
457
458 **Pharmacological assessment of D2R signalling dichotomy**

Eight-week-old C57BL/6 female mice were i.p. injected with the D2R dopamine receptor β-arrestin agonist/Gi antagonist UNC9994 (2 mg/kg; Axon MedChem) or vehicle (10% DMSO; 20% cyclodextrin in saline) and exposed to the "limited access" paradigm or open field test 10 minutes later.

Chemogenetic modulation of D2R neuron activity

Eight-week-old *Drd2*$^{+/+}$ and *Drd2*$^{Cre/+}$ female mice were anesthetized with Ketamine/Xylazine (i.p., 100 mg/kg and 10 mg/kg) and received a Buprenorphine injection (i.p., 0.3 mg/kg) for analgesia. Females were placed on a stereotaxic frame (Kopf Instruments) for subsequent injection of AAV vectors encoding for inhibitory (AAV8-hSYN-DIO-hM4D(Gi)-mCherry; 1.10x10^{13} gc/mL, Addgene) DREADDs. Viruses (300 nL/injection site) were bilaterally injected into the dStri (AP: +1.2mm; ML: +/-1.8mm; DV: -3.5mm) or NAc (AP: +1.5mm; ML: +/-0.7mm; DV: -4.5mm) using a 33-gauge needle connected to a 5 µl Neuro-Syringe (Hamilton). The incision was sutured by VetBondTM (3M) and mice were placed in a heated cage until they recovered from anesthesia. Experiments were conducted 3 weeks later. On experimental days, *Drd2*$^{+/+}$ and *Drd2*$^{Cre/+}$ female mice were i.p. injected with Clozapine-N-oxide (CNO 1 mg/kg; Tocris Bioscience) and exposed to the "limited access" paradigm or open field test 30 minutes later.

Fos immunostaining on AAV8-hSYN- DIO-hM4D(Gi)-mCherry injection sites

Selected 20 µm-thick sections (1 out of 4 sections), throughout the dStri and NAc, of *Drd2*$^{+/+}$ and *Drd2*$^{Cre/+}$ female mice injected with AAV8-hSYN-DIO-hM4D(Gi)-mCherry were blocked with 2% chicken serum in PBS + 0.1% Triton X-100 + 3% BSA and incubated with rabbit anti-Fos antibody (1:500; Synaptic Systems) in blocking solution overnight at 4°C. As secondary antibody, a chicken anti-rabbit Alexa Fluor 488 (1:300; Life Technologies) in PBS + 0.1% Triton X-100 +

3% BSA was used. Imaging was performed using an Olympus fluorescence microscope. The number of Fos+ cells, from 3 animals per genotype, in the dStri and NAc was counted manually using FIJI (ImageJ) software.

Fos/DARPP32 immunostaining on AAV8-hSYN- DIO-hM4D(Gi)-mCherry injection sites

Selected 20 µm-thick sections (1 out of 4 sections), throughout the dStri and NAc, of *Drd2*$^{+/+}$ and *Drd2*$^{Cre/+}$ female mice injected with AAV8-hSYN- DIO-hM4D(Gi)-mCherry were blocked with 2% chicken serum in PBS + 0.1% Triton X-100 + 3% BSA and incubated with rabbit anti-Fos antibody (1:500; Synaptic Systems) and guinea pig anti-DARPP32 antibody (1:1000; Frontier Institute) in blocking solution for 2.5 days at 4°C. As secondary antibodies, a donkey anti-rabbit Alexa Fluor 647 Plus (1:300; Life Technologies) and a donkey anti-guinea pig Alexa Fluor 488 (1:300; Jackson ImmunoResearch) in PBS + 0.1% Triton X-100 + 3% BSA was used. Imaging was performed using a Leica DMI 4000B confocal microscope. The number of Fos+ cells, from 3 animals per genotype, in the dStri and NAc was counted manually using FIJI (ImageJ) software.

Offspring studies: general considerations

Pregnant and lactating dams (n=9 chow-fed and n=11 “limited access” paradigm) underwent weekly follow-ups of body weight and food intake. Litter size was adjusted (between P1-P4) to six-to-eight pups to ensure standardized nutrition until weaning. At weaning, n=1-3 male and female offspring from each litter were randomly subdivided for subsequent studies. For physiological and behavioural tests, the offspring from n=5 chow-fed and n=5 “limited access” paradigm females were used. For compulsive eating predisposition studies, the offspring from n=4 chow-fed and 6 “limited access” paradigm females were used.

Offspring physiological measurements

For glucose tolerance test, mice were i.p. injected with a single bolus of D-glucose (2 g/kg) after 6 hours (P21 animals) (n=8-10 mice/group/sex derived from n=5 dams/group) or overnight (10-week-old) (n=7-8 mice/group/sex derived from n=5 dams/group) fasting. Blood glucose levels were measured using a glucometer (Nova Pro Biomedical).

Compulsive eating predisposition in the offspring

Offspring of mothers continuously submitted to chow diet (n=4) or "limited access" paradigm (n=6) were weaned at 21 days of age. At this time-point, male (n=5/group) and female (n=5/group) pups from both experimental groups were separated and switched to standard chow diet until post-natal day 30. Males and females of similar body weights were submitted to a limited access WD feeding to assess compulsive eating-like behaviour. Briefly, chow and HPF offspring were habituated to WD during 5 days. P35 offspring were exposed to a "limited access" paradigm (2 hours a day, 3 times a week) during 4 weeks without food restriction[11]. Weekly body weight and daily food intake (chow and WD) were measured. The percentage of daily caloric intake consumed during the two hours of intermittent WD access was considered a proxy for compulsive eating behaviour.

Behavioural procedures

Before each test, mice were acclimatized to the behavioural room and arena for 1 hour. The arena was cleaned with 70% ethanol before and after every trial. Light intensity was adapted to each task. A video camera was used to track the movement of each animal. Videos were recorded and analysed with video-tracking software (SMART v3.0, Panlab). For gestational studies, the experiments were conducted in virgins (n=10), pregnant (during the second week of pregnancy)

(n=12) and after pregnancy (n=10) females. For offspring studies, the experiments were conducted in 12-14-week-old male (n=8) and female (n=7-8) offspring from chow (n=7-8 offspring/sex derived from 5 dams) or "limited access" HPF (n=8 offspring/sex derived from 5 dams) mothers.

Open field test

Mice were placed in the centre of a dark methacrylate arena (35x35x35 cm) and allowed to freely explore it for 15 minutes. Animals were tested under a low-intensity light (< 30 lux) to avoid stress. Total distance and the time spent in the corner and centre of the arena was scored.

Dark-light box test

Our protocol was based on previous studies[44]. The test apparatus consisted of a methacrylate arena (35x35x35 cm) divided into a small dark (safe) compartment and a large strongly-illuminated (200 lux; aversive) compartment. A door connected both compartments. Mice were placed in the dark compartment and allowed to freely move between the two chambers for 5 minutes. Video tracking data was analysed to calculate the time spent in each compartment and the latency to enter the illuminated compartment.

Elevated plus maze test

Our protocol was based on previous studies[44]. The apparatus used was a cross-shaped 4-arm maze, with 2 open arms and 2 closed arms (25 x 5 cm). This structure was elevated 60 cm above the floor. Mice were placed in the centre of the apparatus, facing towards a closed arm, and their behaviour was video recorded for 5 minutes. Time spent in the closed arms and open arms was analysed.

555 **Novel object recognition test (NORT)**

556 The novel object recognition test (NORT) was based on Leger and collaborators[45]. The test was
557 conducted in a methacrylate (35x35x35 cm) arena under a 20 lux environment. NORT consisted
558 in three phases: habituation, training and test. During habituation (day 1), mice were allowed to
559 explore the arena for 10 minutes. In the training phase (day 2), mice were allowed to explore two
560 identical objects (equidistantly spaced) for 10 minutes. The test phase was conducted 24 hours
561 later to measure long term memory. In this phase, one of the objects was replaced by a new one
562 and the mouse was allowed to explore them for 10 minutes. The position of the 2 objects was
563 constant across sessions. Discrimination indices were calculated as: $(Time_{novel} - Time_{familiar}) /$
564 $(Time_{novel} + Time_{familiar})$. We also scored total exploratory time $(Time_{novel} + Time_{familiar})$ and total
565 distance travelled. Animals that showed freezing behaviour or exhibiting <5s of exploratory
566 behaviour were excluded. The trial was video-recorded and analysed off-line.

567

568 **Statistical Analysis**

569 Data are expressed as mean ± SEM. Two group-one factor comparisons were performed using a
570 two-tailed unpaired Student's t test. Three groups-one factor comparisons were performed using a
571 one-way ANOVA, and two or three factors comparisons were performed using two-way or three-
572 way ANOVA followed by Tukey's multiple comparison test when computing confidence intervals
573 for every comparison or the Holm-Šídák test when not. Factor results (in relation with the variables
574 Group, Time and/or the interaction Group:Time in the female studies, Fig. 1 Extended Data Fig. 1
575 and Extended Data Fig. 9) are shown next to the graph (lack of this information means that no
576 significant differences were found). For offspring studies (Fig. 4 and Extended Data Fig. 10), we
577 implemented a linear mixed-effects model analysis to account for statistical dependence among
578 individuals originating from the same dam. In the case of non-repeated measures, comparisons

were conducted between experimental "diet" and offspring "sex" (fixed effects), while setting the variable "dam" as a random term. For physiological and compulsive-eating predisposition studies, when repeated measurements were recorded over time, comparisons were made between "diet", offspring "sex" and "time" of record (fixed effects). The variables "dam" and "pup ID" were considered as random factors. The statistical significance of experimental treatments was assessed by an analysis of deviance (ANODE). Given the substantial number of statistical comparisons involved in the compulsive eating study, all p values were adjusted using the Benjamini–Yekutieli test thus minimizing the false discovery rate. Results from all post-hoc analysis are depicted on top of the graph bars using asterisks. Z-scores were calculated by dividing the difference between the individual data determined in each experiment (x) and the mean of the control group (m), to the standard deviation of the control group (s) ($z=(x-m)/s$). We defined chow diet as the control group. Complementary measures (open field, dark-light box, and elevated plus maze) were integrated by implementing a z-normalization across diverse behavioural tests as previously described[22]. Analysis was performed with Graphpad v8 and R v4.0.2 (lme4, car and multcomp packages) softwares. $P<0.05$ was considered significant.

Acknowledgments: We are grateful to Josep Maria Marimon (Universitat de Barcelona) for mouse vasectomy procedures; Ainhoa Garcia (IDIBAPS) for assistance with mouse breeding; Dr. Serge Luquet (Université de Paris), Dr. Albert Quintana (Universitat Autònoma de Barcelona) and Dr. Marc Schneeberger (Yale University) for valuable comments on the manuscript. This work was supported by: the European Research Council (ERC) under the European Union's Horizon 2020 research and innovation programme (Grant agreement No. 725004), ''la Caixa'' Foundation (ID100010434) under agreement LCF/PR/HR19/52160016 and the CERCA Programme/Generalitat de Catalunya (M.C.); Grant PID2019-105136RB-100, Spanish Ministry of Economy and Competitiveness (MINECO) and European Regional Development Fund (ERDF) (A.B.); Marie Skłodowska-Curie Action fellowship (H2020-MSCA-IF) NEUROPREG (Grant agreement No. 891247) (R.H-T.); the Spanish Ministry of Science and Innovation, Juan de la Cierva fellowship (IJC2018-037341-I) (S.R.); Miguel Servet contract (CP19/00083) from Instituto de Salud Carlos III co-financed by ERDF (A.O.). This work was carried out in part at Esther Koplowitz Centre.

Author contributions R.H-T. and M.C. conceptualized and supervised the study, and acquired project funding. M.C. administered the project. R.H-T., S.R., M.M-G., M.P., I.C., A.O., A.G.G-V., M.T., E.E., L.M-R., J.A., A.B. performed experiments and discussed data. E.M-M. and G.S. performed fMRI data acquisition and analyses. R.H-T., S.R., E.M-M., E.V., G.S., L.M-R., A.B. and M.C. contributed to method development and data interpretation. R.H-T., E.M-M., G.S. and M.C. developed the data visualizations. R.H-T. and M.C. wrote the original draft of the paper with editing and reviewing inputs from all authors.

Competing interests: Authors declare no competing interests.

Data availability: All data are available in the main text or the supplementary information, including Source Data. The data that support the findings of the study are available from the corresponding authors upon reasonable request.

623 **References**

624 1. Talbot, L. & Maclennan, K. Physiology of pregnancy. *Anaesth. Intensive Care Med.* **17**, 341–
625 345 (2016).
626 2. Orloff, N. C. & Hormes, J. M. Pickles and ice cream! Food cravings in pregnancy: hypotheses,
627 preliminary evidence, and directions for future research. *Front. Psychol.* **5**, (2014).
628 3. Orloff, N. C. *et al.* Food cravings in pregnancy: Preliminary evidence for a role in excess
629 gestational weight gain. *Appetite* **105**, 259–265 (2016).
630 4. Fontaine, E. Food intake and nutrition during pregnancy, lactation and weaning in the dam and
631 offspring. *Reprod. Domest. Anim. Zuchthyg.* **47 Suppl 6**, 326–330 (2012).
632 5. Hadjieconomou, D. *et al.* Enteric neurons increase maternal food intake during reproduction.
633 *Nature* **587**, 455–459 (2020).
634 6. Speakman, J. R. The physiological costs of reproduction in small mammals. *Philos. Trans. R.*
635 *Soc. B Biol. Sci.* **363**, 375–398 (2008).
636 7. Bodden, C., Hannan, A. J. & Reichelt, A. C. Of 'junk food' and 'brain food': how parental
637 diet influences offspring neurobiology and behaviour. *Trends Endocrinol. Metab. TEM* (2021)
638 doi:10.1016/j.tem.2021.04.001.
639 8. Schoonejans, J. M. & Ozanne, S. E. Developmental programming by maternal obesity:
640 Lessons from animal models. *Diabet. Med.* **38**, (2021).
641 9. Hasebe, K., Kendig, M. D. & Morris, M. J. Mechanisms Underlying the Cognitive and
642 Behavioural Effects of Maternal Obesity. *Nutrients* **13**, 240 (2021).
643 10. Todman, D. Soranus of Ephesus (AD 98–138) and the Methodist sect. *J. Med. Biogr.* **16**, 51–
644 51 (2008).
645 11. Schroeder, M. *et al.* A Methyl-Balanced Diet Prevents CRF-Induced Prenatal Stress-Triggered
646 Predisposition to Binge Eating-like Phenotype. *Cell Metab.* **25**, 1269-1281.e6 (2017).

12. Hook, E. B. Dietary cravings and aversions during pregnancy. *Am. J. Clin. Nutr.* **31**, 1355–1362 (1978).
13. Rosenbaum, D. L. & White, K. S. The Role of Anxiety in Binge Eating Behavior: A Critical Examination of Theory and Empirical Literature. *Health Psychol. Res.* **1**, e19 (2013).
14. Ferrario, C. R. *et al.* Homeostasis Meets Motivation in the Battle to Control Food Intake. *J. Neurosci.* **36**, 11469–11481 (2016).
15. Andermann, M. L. & Lowell, B. B. Toward a Wiring Diagram Understanding of Appetite Control. *Neuron* **95**, 757–778 (2017).
16. Grandjean, J. *et al.* Common functional networks in the mouse brain revealed by multi-centre resting-state fMRI analysis. *NeuroImage* **205**, 116278 (2020).
17. Beaulieu, J.-M. & Gainetdinov, R. R. The Physiology, Signaling, and Pharmacology of Dopamine Receptors. *Pharmacol. Rev.* **63**, 182–217 (2011).
18. Lindgren, N. *et al.* Dopamine D_2 receptors regulate tyrosine hydroxylase activity and phosphorylation at Ser40 in rat striatum: D_2 -mediated regulation of TH in striatum. *Eur. J. Neurosci.* **13**, 773–780 (2001).
19. Azevedo, E. P. *et al.* A Role of Drd2 Hippocampal Neurons in Context-Dependent Food Intake. *Neuron* **102**, 873-886.e5 (2019).
20. Luo, Y.-J. *et al.* Nucleus accumbens controls wakefulness by a subpopulation of neurons expressing dopamine D1 receptors. *Nat. Commun.* **9**, 1576 (2018).
21. Jendryka, M. *et al.* Pharmacokinetic and pharmacodynamic actions of clozapine-N-oxide, clozapine, and compound 21 in DREADD-based chemogenetics in mice. *Sci. Rep.* **9**, 4522 (2019).

22. Allen, J. A. *et al.* Discovery of -Arrestin-Biased Dopamine D2 Ligands for Probing Signal Transduction Pathways Essential for Antipsychotic Efficacy. *Proc. Natl. Acad. Sci.* **108**, 18488–18493 (2011).
23. Urs, N. M. *et al.* Distinct cortical and striatal actions of a β-arrestin–biased dopamine D2 receptor ligand reveal unique antipsychotic-like properties. *Proc. Natl. Acad. Sci.* **113**, E8178–E8186 (2016).
24. Guilloux, J.-P., Seney, M., Edgar, N. & Sibille, E. Integrated behavioral z-scoring increases the sensitivity and reliability of behavioral phenotyping in mice: Relevance to emotionality and sex. *J. Neurosci. Methods* **197**, 21–31 (2011).
25. Treasure, J., Duarte, T. A. & Schmidt, U. Eating disorders. *The Lancet* **395**, 899–911 (2020).
26. Lippert, R. N. *et al.* Maternal high-fat diet during lactation reprograms the dopaminergic circuitry in mice. *J. Clin. Invest.* **130**, 3761–3776 (2020).
27. Peleg-Raibstein, D. *et al.* Enhanced sensitivity to drugs of abuse and palatable foods following maternal overnutrition. *Transl. Psychiatry* **6**, e911 (2016).
28. Blau, L. E., Orloff, N. C., Flammer, A., Slatch, C. & Hormes, J. M. Food craving frequency mediates the relationship between emotional eating and excess weight gain in pregnancy. *Eat. Behav.* **31**, 120–124 (2018).
29. Volkow, N. D., Wise, R. A. & Baler, R. The dopamine motive system: implications for drug and food addiction. *Nat. Rev. Neurosci.* **18**, 741–752 (2017).
30. Caravaggio, F. *et al.* Ventral striatum binding of a dopamine D2/3 receptor agonist but not antagonist predicts normal body mass index. *Biol. Psychiatry* **77**, 196–202 (2015).
31. Eisenstein, S. A. *et al.* Emotional Eating Phenotype is Associated with Central Dopamine D2 Receptor Binding Independent of Body Mass Index. *Sci. Rep.* **5**, 11283 (2015).

32. Domingo-Rodriguez, L. *et al.* A specific prelimbic-nucleus accumbens pathway controls resilience versus vulnerability to food addiction. *Nat. Commun.* **11**, 782 (2020).
33. Seeley, W. W. The Salience Network: A Neural System for Perceiving and Responding to Homeostatic Demands. *J. Neurosci.* **39**, 9878–9882 (2019).
34. Naqvi, N. H., Rudrauf, D., Damasio, H. & Bechara, A. Damage to the Insula Disrupts Addiction to Cigarette Smoking. *Science* **315**, 531–534 (2007).
35. Faas, M. M., Melgert, B. N. & de Vos, P. A Brief Review on How Pregnancy and Sex Hormones Interfere with Taste and Food Intake. *Chemosens. Percept.* **3**, 51–56 (2010).
36. Yoest, K. E., Quigley, J. A. & Becker, J. B. Rapid effects of ovarian hormones in dorsal striatum and nucleus accumbens. *Horm. Behav.* **104**, 119–129 (2018).
37. Gong, S. *et al.* Targeting Cre Recombinase to Specific Neuron Populations with Bacterial Artificial Chromosome Constructs. *J. Neurosci.* **27**, 9817–9823 (2007).
38. Puighermanal, E. *et al.* Functional and molecular heterogeneity of D2R neurons along dorsal ventral axis in the striatum. *Nat. Commun.* **11**, 1957 (2020).
39. Sclafani, A., Zukerman, S. & Ackroff, K. Postoral glucose sensing, not caloric content, determines sugar reward in C57BL/6J mice. *Chem. Senses* **40**, 245–258 (2015).
40. Domingos, A. I. *et al.* Leptin regulates the reward value of nutrient. *Nat. Neurosci.* **14**, 1562–1568 (2011).
41. Nickerson, L. D., Smith, S. M., Öngür, D. & Beckmann, C. F. Using Dual Regression to Investigate Network Shape and Amplitude in Functional Connectivity Analyses. *Front. Neurosci.* **11**, (2017).
42. Timper, K. *et al.* Mild Impairment of Mitochondrial OXPHOS Promotes Fatty Acid Utilization in POMC Neurons and Improves Glucose Homeostasis in Obesity. *Cell Rep.* **25**, 383-397.e10 (2018).

716 43. Altarche-Xifro, W. *et al.* Functional Rescue of Dopaminergic Neuron Loss in Parkinson's
717 Disease Mice After Transplantation of Hematopoietic Stem and Progenitor Cells.
718 *EBioMedicine* **8**, 83–95 (2016).
719 44. Fan, K. *et al.* Stress-Induced Metabolic Disorder in Peripheral CD4+ T Cells Leads to Anxiety-
720 like Behavior. *Cell* **179**, 864-879.e19 (2019).
721 45. Leger, M. *et al.* Object recognition test in mice. *Nat. Protoc.* **8**, 2531–2537 (2013).
722
723 Correspondence and request for materials should be addressed to: mclaret@clinic.cat;
724 haddad@clinic.cat.
725

Figure Legends

Fig. 1 | Sweet taste perception and food craving-like behaviour increase during pregnancy. **a**, Schematic illustration of two-bottle paradigm and experimental timeline. **b-c**, Sucralose (0.05 mM) preference (**b**) and area under the curve (AUC) (**c**) throughout the study of virgin (n=5), pseudopregnant (n=5) and pregnant mice (n=5). **d-e,** Sucrose (25 mM) preference (**d**) and area under the curve (AUC) (**e**) throughout the study of virgin (n=5), pseudopregnant (n=5) and pregnant mice (n=5). **f**, Schematic illustration of the "limited access" paradigm and experimental timeline. **g**, Percentage of daily caloric intake, consumed during the 2-hours of HPF access throughout the study, of virgin (n=8), pseudopregnant (n=22) and pregnant (n=13) mice. Dots in all panels represent individual sample data. Data are expressed as mean ± SEM. Exact P values are shown. One-way ANOVA with Tukey's multiple comparisons test was performed for **c** and **e,** two-way ANOVA with Dunnett's multiple comparisons test for **b**, **d** and two-way ANOVA with Tukey's multiple comparisons test for **g**. When the factors Group, Time and/or the interaction Group:Time were considered significant, results are shown with the significant factor or the interaction effect next to it (**b**, **d**). *BP: before pregnancy; W1: first week of pregnancy (or concomitant experimental week for virgins and pseudopregnants); W2: second week of pregnancy (or concomitant experimental week for virgins and pseudopregnants); W3: third week of pregnancy (or concomitant experimental week for virgins and pseudopregnants); AP: after pregnancy.*

Fig. 2 | Brain functional networks related to reward and emotions are transiently increased during pregnancy. **a**, Schematic illustration of fMRI experimental timeline. **b**, Shape and amplitude analysis of the cortico-striatal network in virgins (n=7), pregnants (n=8) and after pregnancy (n=9). **c**, Coronal slices of whole-brain spatial map of the cortico-striatal network,

including reward and motor control areas. Axial (above, left) and sagittal (below, left) representative slices of the independent component spatial map are shown. **d**, Shape and amplitude analysis of the salience network in virgins (n=7), pregnants (n=8) and after pregnancy (n=9). **e**, Coronal slices of whole-brain spatial map of the salience network including gustatory, motor, limbic and dopaminergic control areas. Axial (above, left) and sagittal (above, right) representative slices of the independent component spatial map are shown. Dots in all panels represent individual sample data. Data are expressed as mean ± SEM. Exact P values are shown. Statistical analysis was performed by Kruskal-Wallis test. *IL: infralimbic cortex; Ins: insula; MCx: motor cortex; Pir: pririform cortex; PrL: prelimbic cortex; SCx: sensory cortex; S: septum; Stri: dorsal and ventral striatum; VCx: visual cortex; vMB: ventral midbrain.*

Fig. 3 | Accumbal D2R neurons underlie pregnancy-specific food craving-like behaviour. a, NAc *Drd1* mRNA particles per neuron (n=6 mice/group). **b**, Percentage of NAc *Fos* positive *Drd1* neurons (n=6 mice/group). **c**, NAc *Drd2* mRNA particles per neuron (n=6 mice/ group). **d**, Percentage of NAc *Fos* positive *Drd2* neurons (n=6 mice/group). **e**, Schematic illustration of pre- and postsynaptic D2R-specific signalling in the striatum. Phosphorylation status is depicted by red circle. **f**, NAc immunoblot assessing TH phosphorylation levels at residues Ser31 (p-TH^{S31}) and Ser40 (p-TH^{S40}) (n=5 mice/group). **g**, NAc immunoblot assessing G protein-dependent and non-canonical β−arrestin-dependent signalling pathways showing its downstream targets, DARPP-32 phosphorylation levels (at residue pThr34; p-D-32^{T34}) and GSK3β phosphorylation levels (at residue pSer9; p-GSK3β^{S9}), respectively (n=5 mice/group). **h-i,** NAc neurotransmitter (DA, DOPAC and HVA) levels (**h**), dopamine turnover (DOPAC to DA ratio) and dopamine storage (HVA to DA ratio) (**i**) of virgins (n=9) and pregnant (n=8) females. **j-k**, Schematic illustration of the experimental strategy (left) and percentage of daily caloric intake (right) consumed during the

2-hours of HPF access of female mice injected with hM4D(Gi) in the NAc (n=7 *Drd2*$^{+/+}$ and 5 *Drd2*$^{Cre/+}$) and in the dStri (n=4 *Drd2*$^{+/+}$ and 3 *Drd2*$^{Cre/+}$) before and during the second week of pregnancy. Dots in all panels represent individual sample data. Data are expressed as mean ± SEM. Exact P values are shown. Statistical analysis was performed by one-way ANOVA with Tukey's multiple comparisons test for **a**, **b**, **c**, **d**, **f**, **g** and by two-way ANOVA with Sidak's multiple comparisons test for **h**, **i, j, k**. *NAc: nucleus accumbens; Drd1: dopamine receptor 1; Drd2: dopamine receptor 2; Th: tyrosine hydroxylase; DA: dopamine; PKA: protein kinase A; DARPP-32: dopamine- and cAMP-regulated phosphoprotein; Gsk3β: glycogen synthase kinase 3 beta, Mr 32 kDa; DOPAC: 3,4-Dihydroxyphenylacetic acid; HVA: homovanillic acid; dStri: dorsal striatum; V: virgins; P: pregnants; AP: after pregnancy; BP: before pregnancy; W2: second week of pregnancy.*

Fig. 4 | Recurrent maternal HPF craving-like behaviour deteriorates offspring health. a, Body weight at P21 of male (n=9 Chow-O and 11 HPF-O) and female (n=8 Chow-O and 12 HPF-O) offspring born to mothers fed with chow (Chow-O) (n=5) or HPF (HPF-O) (n=5). **b,** GTT of P21 male (n=9 Chow-O and 10 HPF-O) (left panel) and female (n=8 Chow-O and 9 HPF-O) Chow-O (n=5) or HPF-O (n=5). **c,** Body weight of 12-week-old male (n=8 mice/group) and female (n=7 Chow-O and 8 HPF-O) Chow-O (n=5) or HPF (HPF-O) (n=5). **d,** gWAT weight normalized by total body mass in male (n=8 Chow-O and 7 HPF-O) and female (n=7 Chow-O and 8 HPF-O) Chow-O (n=5) or HPF-O (n=5). **e,** GTT of 10-week-old male (n=8 mice/group) and female (n=7 Chow-O and 8 HPF-O) Chow-O (n=5) or HPF (HPF-O) (n=5). **f-g**, Open field performance in 12-week-old male (n=8 mice/group) and female (n=7 Chow-O and 8 HPF-O) Chow-O (n=5) or HPF (HPF-O) (n=5), including time spent per zone (**f**, corner and **g**, center) and (**h**) representative traces. **i,** Time spent in the light compartment in 12-week-old male (n=8 mice/group) and female (n=7

798 Chow-O and 8 HPF-O) Chow-O (n=5) or HPF-O (n=5). **j**, Time spent in the open arm in 12-week-
799 old male (n=8 mice/group) and female (n=7 Chow-O and 8 HPF-O) Chow-O (n=5) or HPF-O
800 (n=5). **k**, Anxiety score (male n=8 mice/group and female n=7 Chow-O and 8 HPF-O) after z-
801 normalization of the different behavioural anxiety paradigms shown in **g**, **i**, **j**. **l-n**, Long term
802 memory parameters in Chow-O and HPF-O 13-week-old male (n=8 mice/group) and female (n=7
803 Chow-O and 8 HPF-O) mice, including discrimination index (**l**), exploratory time (**m**), and
804 representative traces (**n**). Blue circle and red square depict familiar and unfamiliar objects,
805 respectively. **o**, Percentage of daily caloric intake, consumed during the 2-hours of HPF access
806 throughout adolescence, in Chow-O and HPF-O male and female mice (n=5 mice per group/
807 average of 3 measurements per week). Dots in all panels represent individual sample data. Data
808 are expressed as mean ± SEM. Statistical analysis was performed by ANODE for **a**, **b, c**, **d**, **e, f**,
809 **g**, **i**, **j**, **k**, **l**, **m** or ANODE followed by Benjamini–Yekutieli adjustment for **o**. When the factors
810 Sex, Diet, Time and/or the interaction Sex:Diet, Sex:Time, Diet:Time, Sex:Diet:Time were
811 considered significant, results were shown with significant factor or the interaction effect with
812 Tukey's post-hoc analysis within the same sex group. Exact P values are shown.

Figure 1

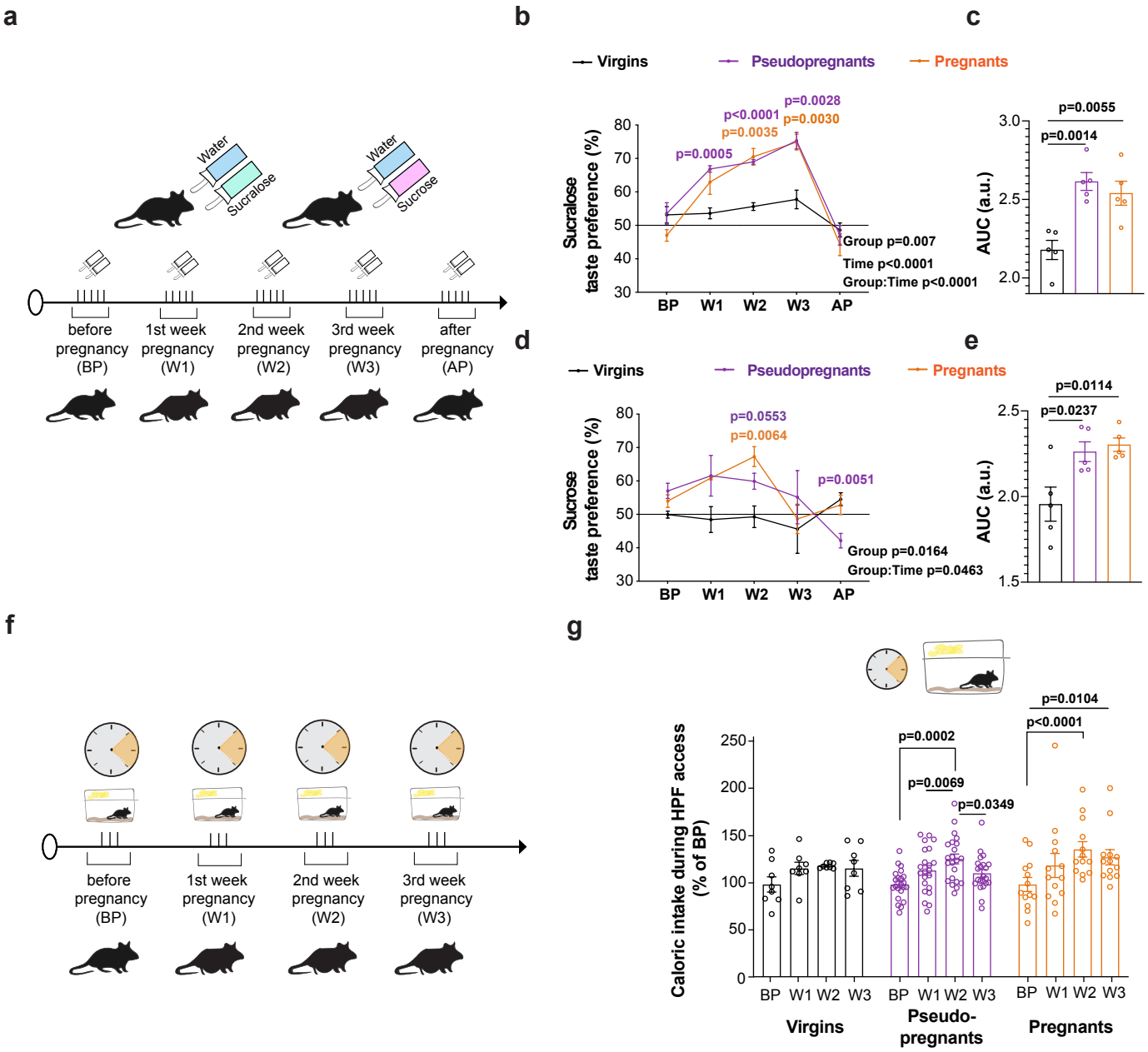
a
Water
Sucralose
Water
Sucrose
before pregnancy (BP)
1st week pregnancy (W1)
2nd week pregnancy (W2)
3rd week pregnancy (W3)
after pregnancy (AP)
b
Virgins
Pseudopregnants
Pregnants
Sucralose taste preference (%)
p=0.0005
p<0.0001
p=0.0035
p=0.0028
p=0.0030
Group p=0.007
Time p<0.0001
Group:Time p<0.0001
BP W1 W2 W3 AP
c
AUC (a.u.)
p=0.0055
p=0.0014
d
Virgins
Pseudopregnants
Pregnants
Sucrose taste preference (%)
p=0.0553
p=0.0064
p=0.0051
Group p=0.0164
Group:Time p=0.0463
BP W1 W2 W3 AP
e
AUC (a.u.)
p=0.0114
p=0.0237
f
before pregnancy (BP)
1st week pregnancy (W1)
2nd week pregnancy (W2)
3rd week pregnancy (W3)
g
Caloric intake during HPF access (% of BP)
p=0.0002
p=0.0069
p=0.0349
p=0.0104
p<0.0001
BP W1 W2 W3 BP W1 W2 W3 BP W1 W2 W3
Virgins
Pseudo-pregnants
Pregnants

Figure 2

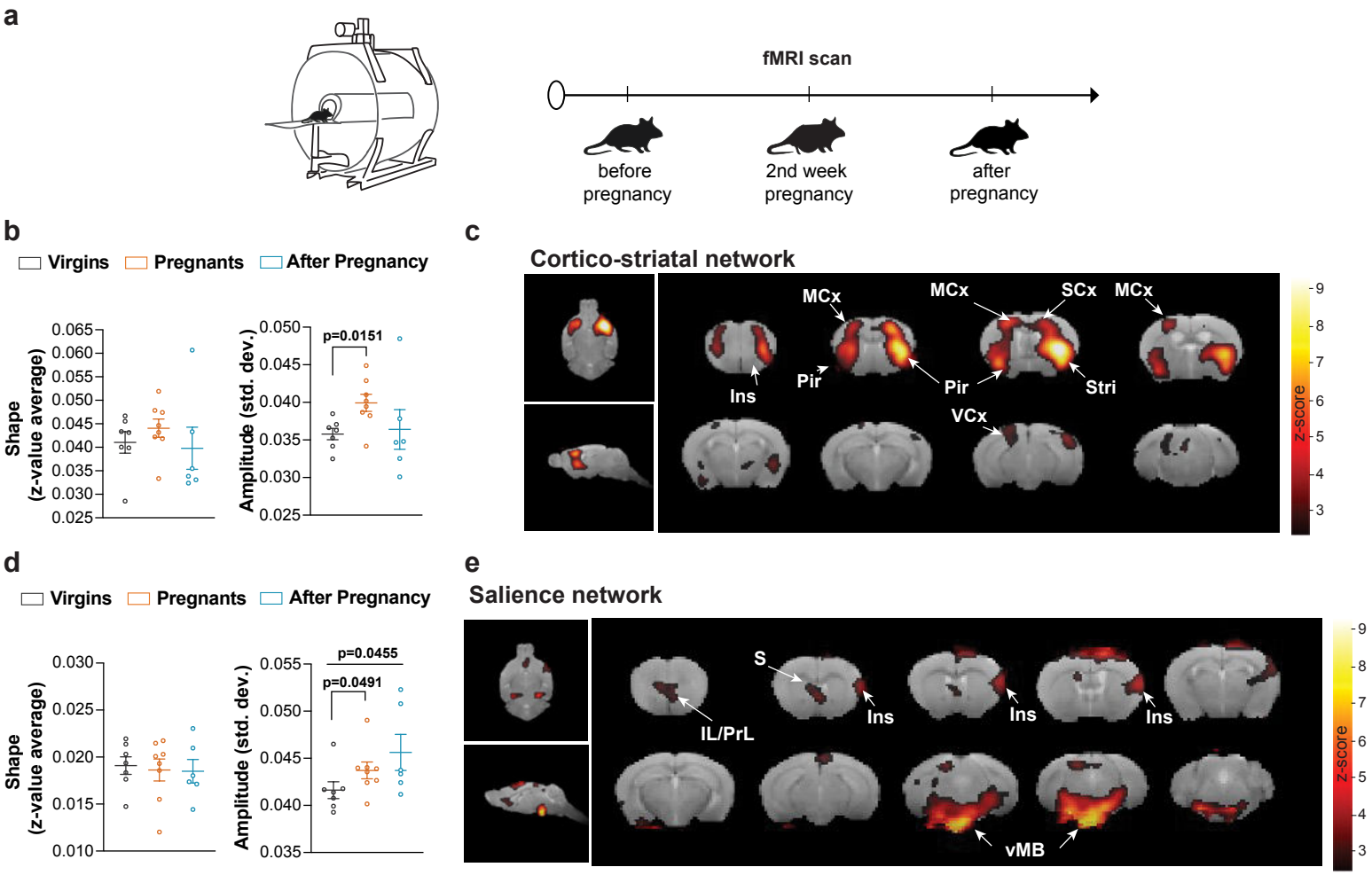
a
fMRI scan
before pregnancy
2nd week pregnancy
after pregnancy
b
Virgins
Pregnants
After Pregnancy
Shape (z-value average)
Amplitude (std. dev.)
p=0.0151
c
Cortico-striatal network
MCx
SCx
Ins
Pir
Stri
VCx
z-score
d
Virgins
Pregnants
After Pregnancy
Shape (z-value average)
Amplitude (std. dev.)
p=0.0455
p=0.0491
e
Salience network
S
Ins
IL/PrL
vMB
z-score

Figure 3

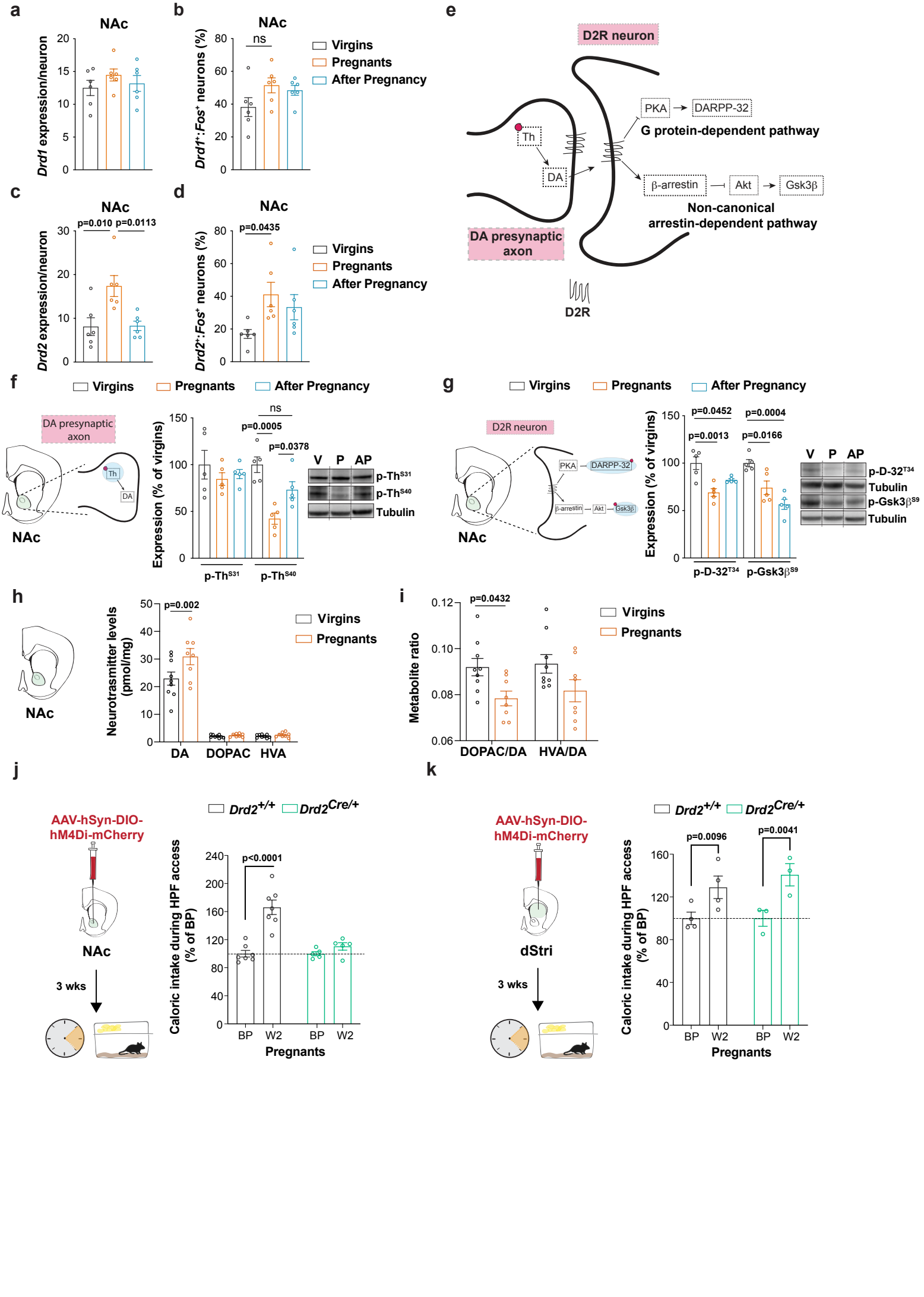
a
NAc
Drd1 expression/neuron
b
NAc
ns
Drd1+:Fos+ neurons (%)
Virgins
Pregnants
After Pregnancy
e
D2R neuron
PKA
DARPP-32
G protein-dependent pathway
Th
DA
β-arrestin
Akt
Gsk3β
Non-canonical arrestin-dependent pathway
DA presynaptic axon
D2R
c
NAc
p=0.010 p=0.0113
Drd2 expression/neuron
d
NAc
p=0.0435
Drd2+:Fos+ neurons (%)
Virgins
Pregnants
After Pregnancy
f
Virgins
Pregnants
After Pregnancy
DA presynaptic axon
Th
DA
NAc
ns
p=0.0005
p=0.0378
Expression (% of virgins)
V P AP
p-ThS31
p-ThS40
Tubulin
p-ThS31
p-ThS40
g
Virgins
Pregnants
After Pregnancy
D2R neuron
PKA
DARPP-32
β-arrestin
Akt
Gsk3β
NAc
p=0.0452
p=0.0004
p=0.0013
p=0.0166
Expression (% of virgins)
V P AP
p-D-32T34
Tubulin
p-Gsk3βS9
Tubulin
p-D-32T34
p-Gsk3βS9
h
NAc
p=0.002
Neurotrasmitter levels (pmol/mg)
Virgins
Pregnants
DA
DOPAC
HVA
i
p=0.0432
Metabolite ratio
Virgins
Pregnants
DOPAC/DA
HVA/DA
j
AAV-hSyn-DIO-hM4Di-mCherry
NAc
3 wks
Drd2+/+
Drd2Cre/+
p<0.0001
Caloric intake during HPF access (% of BP)
BP
W2
BP
W2
Pregnants
k
AAV-hSyn-DIO-hM4Di-mCherry
dStri
3 wks
Drd2+/+
Drd2Cre/+
p=0.0096
p=0.0041
Caloric intake during HPF access (% of BP)
BP
W2
BP
W2
Pregnants

Figure 4

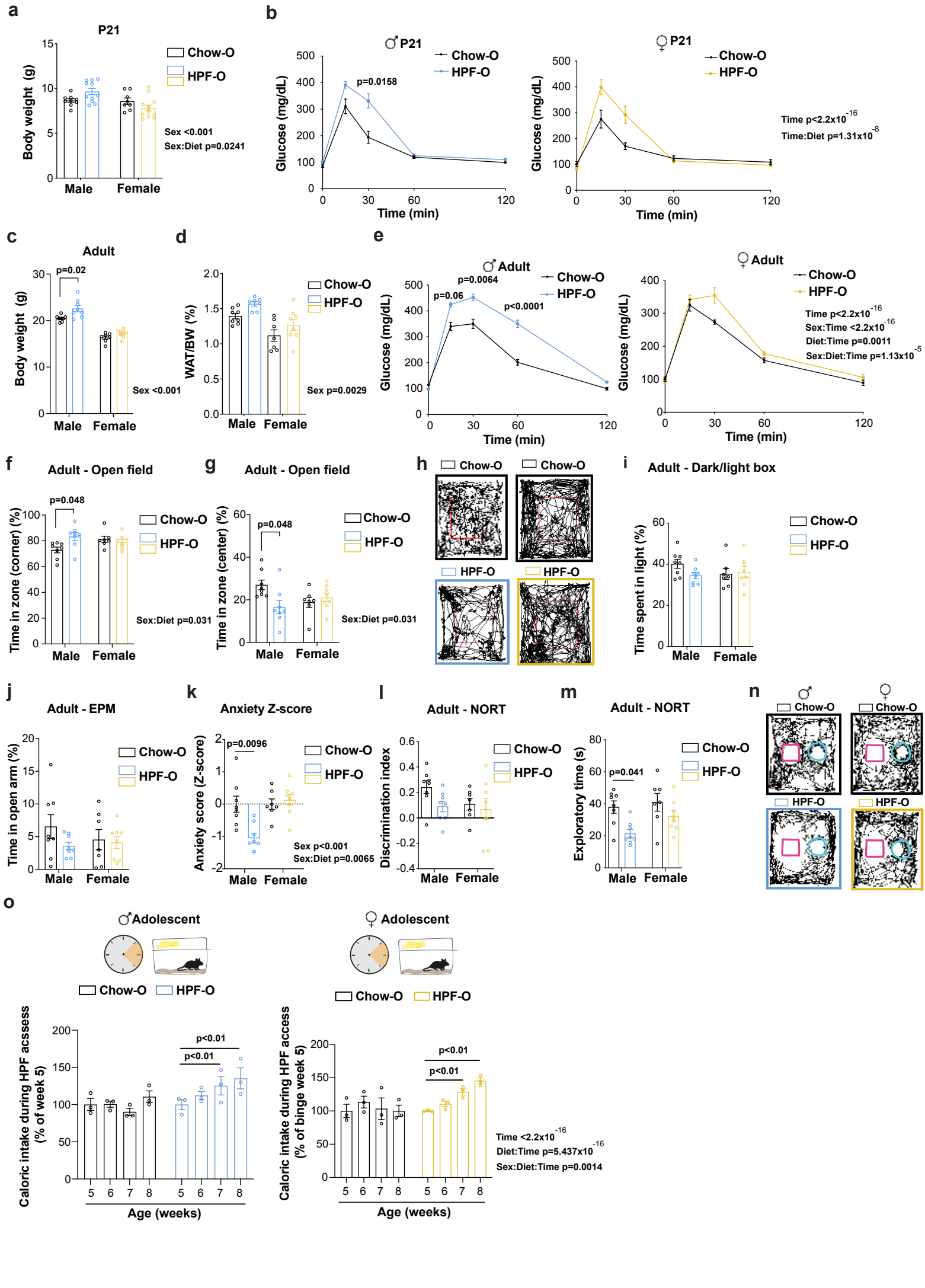
a
P21
Body weight (g)
Chow-O
HPF-O
Sex <0.001
Sex:Diet p=0.0241
Male
Female
b
♂P21
Glucose (mg/dL)
p=0.0158
Time (min)
♀P21
Time p<2.2x10-16
Time:Diet p=1.31x10-8
c
Adult
p=0.02
Sex <0.001
d
WAT/BW (%)
Sex p=0.0029
e
♂Adult
p=0.06
p=0.0064
p<0.0001
♀Adult
Time p<2.2x10-16
Sex:Time <2.2x10-16
Diet:Time p=0.0011
Sex:Diet:Time p=1.13x10-5
f
Adult - Open field
Time in zone (corner) (%)
p=0.048
Sex:Diet p=0.031
g
Time in zone (center) (%)
h
i
Adult - Dark/light box
Time spent in light (%)
j
Adult - EPM
Time in open arm (%)
k
Anxiety Z-score
Anxiety score (Z-score)
p=0.0096
Sex p<0.001
Sex:Diet p=0.0065
l
Adult - NORT
Discrimination index
m
Exploratory time (s)
p=0.041
n
o
♂Adolescent
♀Adolescent
Caloric intake during HPF accsess (% of week 5)
p<0.01
Age (weeks)
Caloric intake during HPF access (% of binge week 5)
Time <2.2x10-16
Diet:Time p=5.437x10-16
Sex:Diet:Time p=0.0014

Extended Data Figure 1

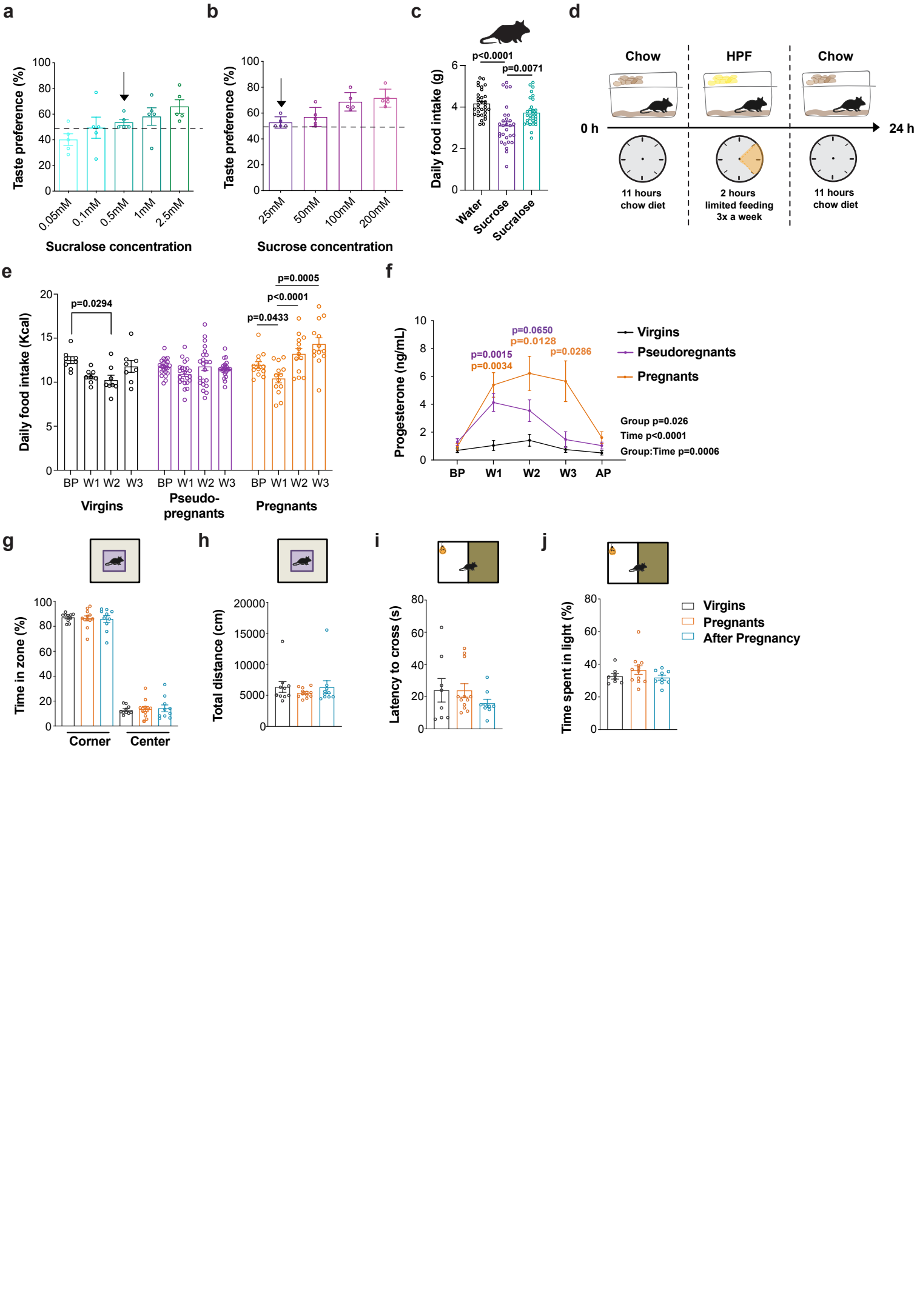

Extended Data Figure 2

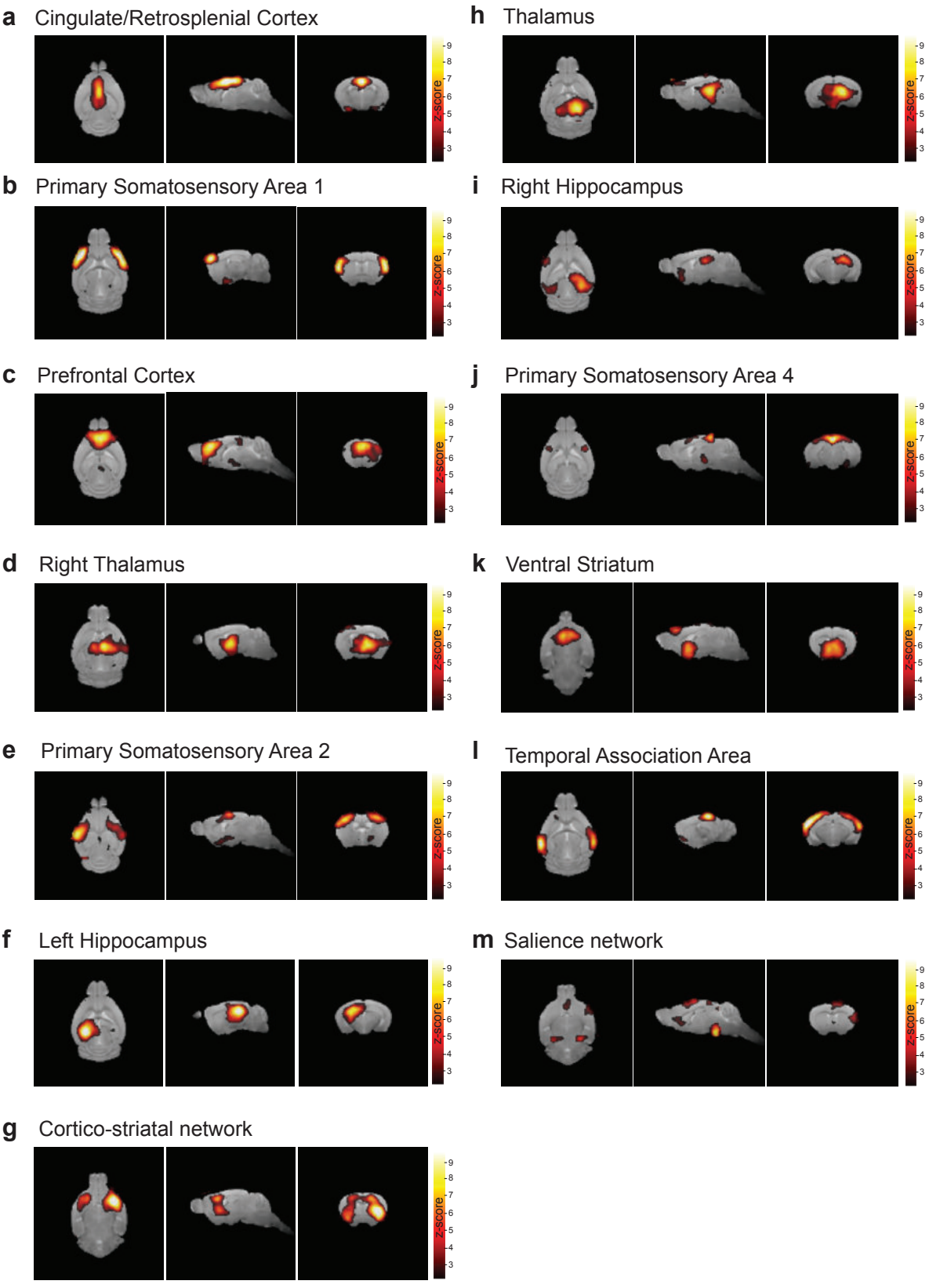

Extended Data Figure 3

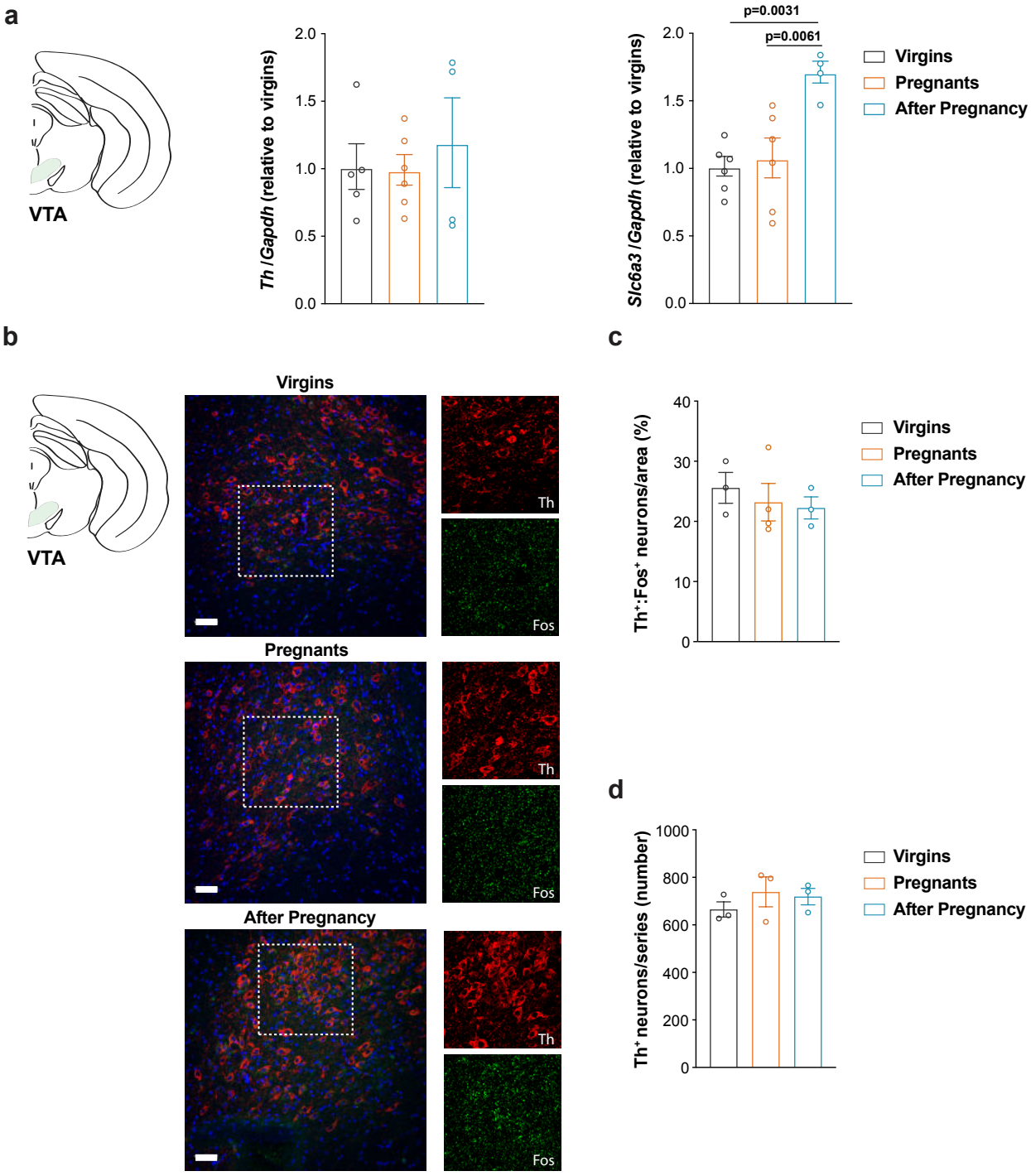

Extended Data Figure 4

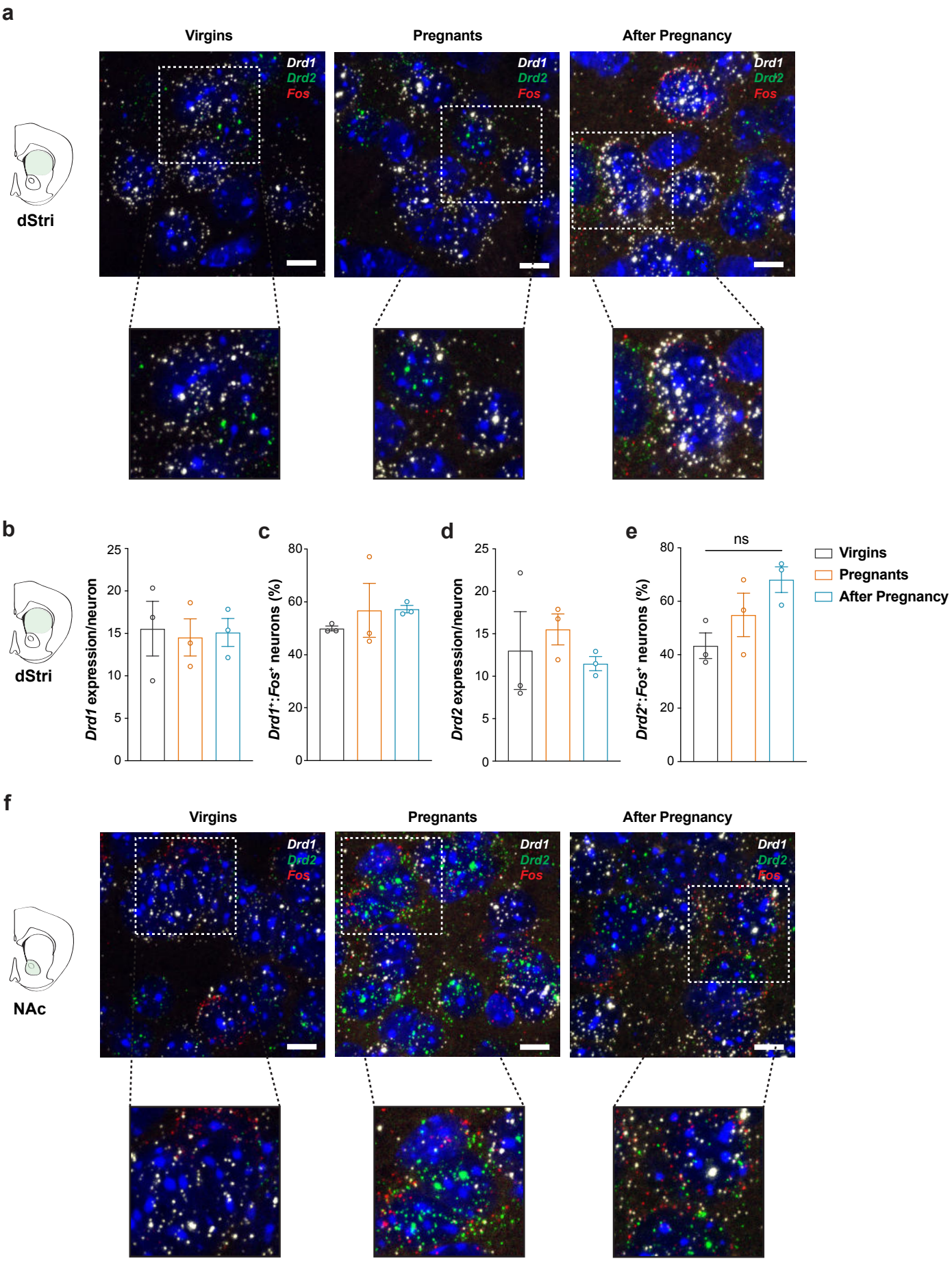

Extended Data Figure 5

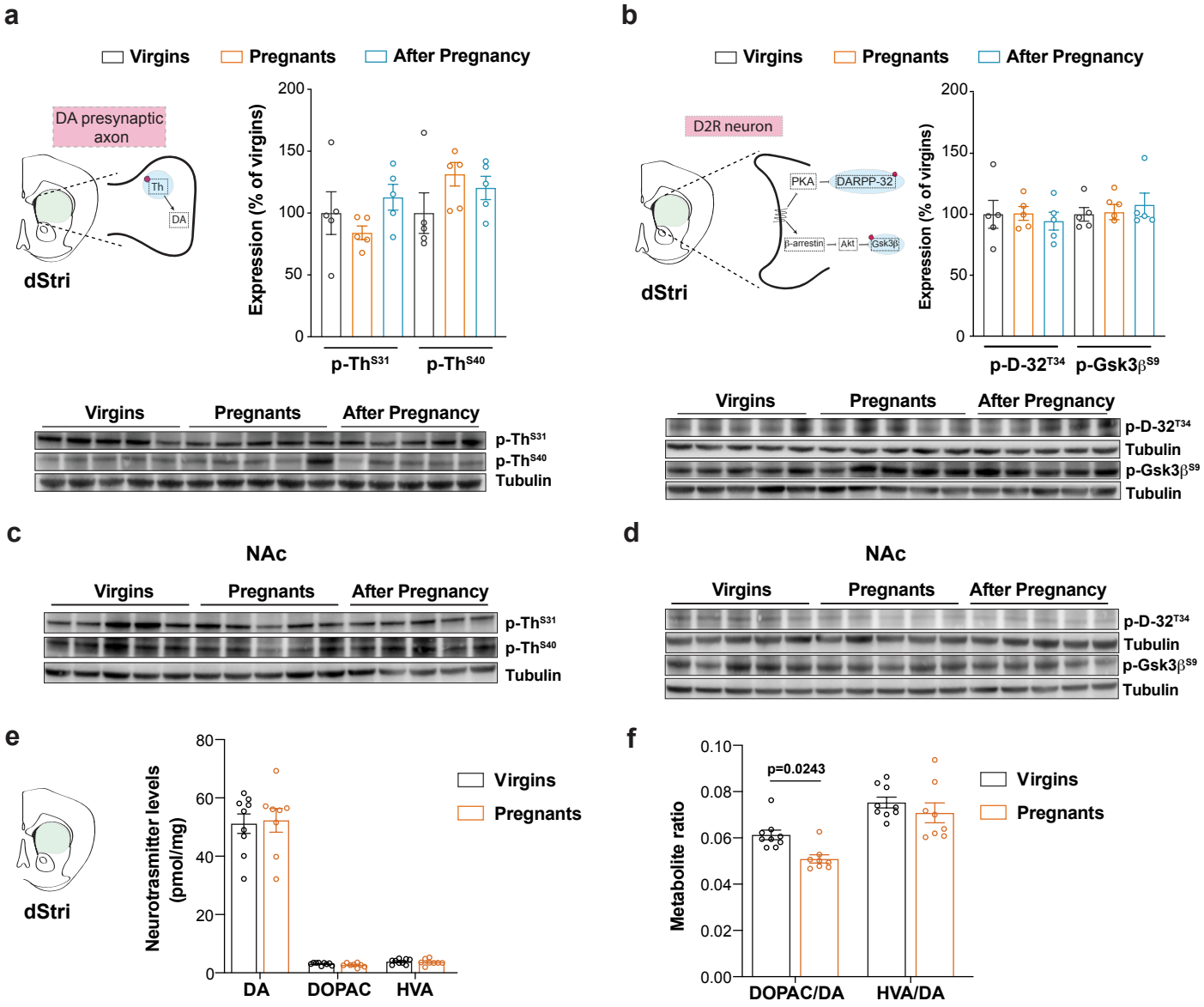

Extended Data Figure 6

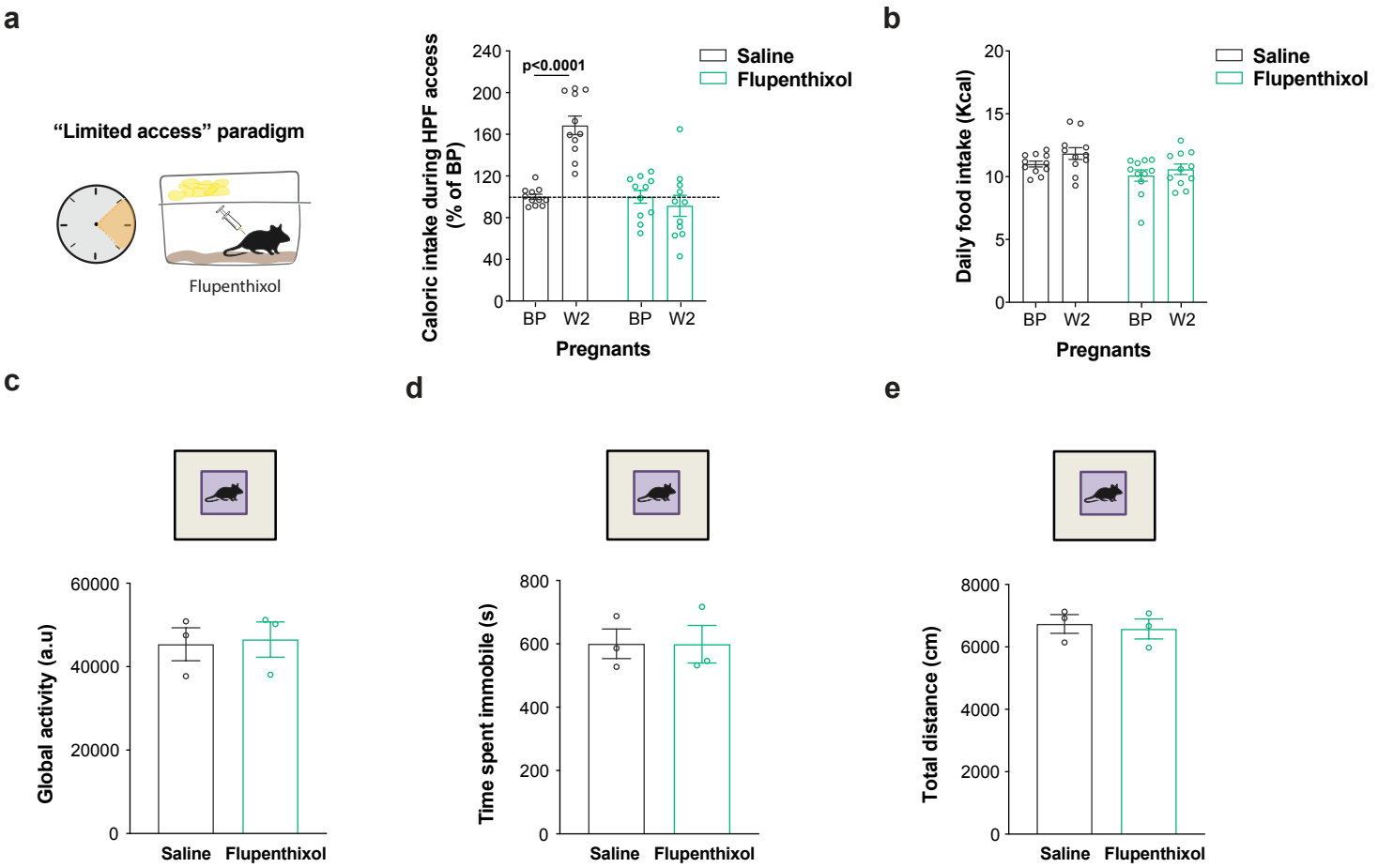

Extended Data Figure 7

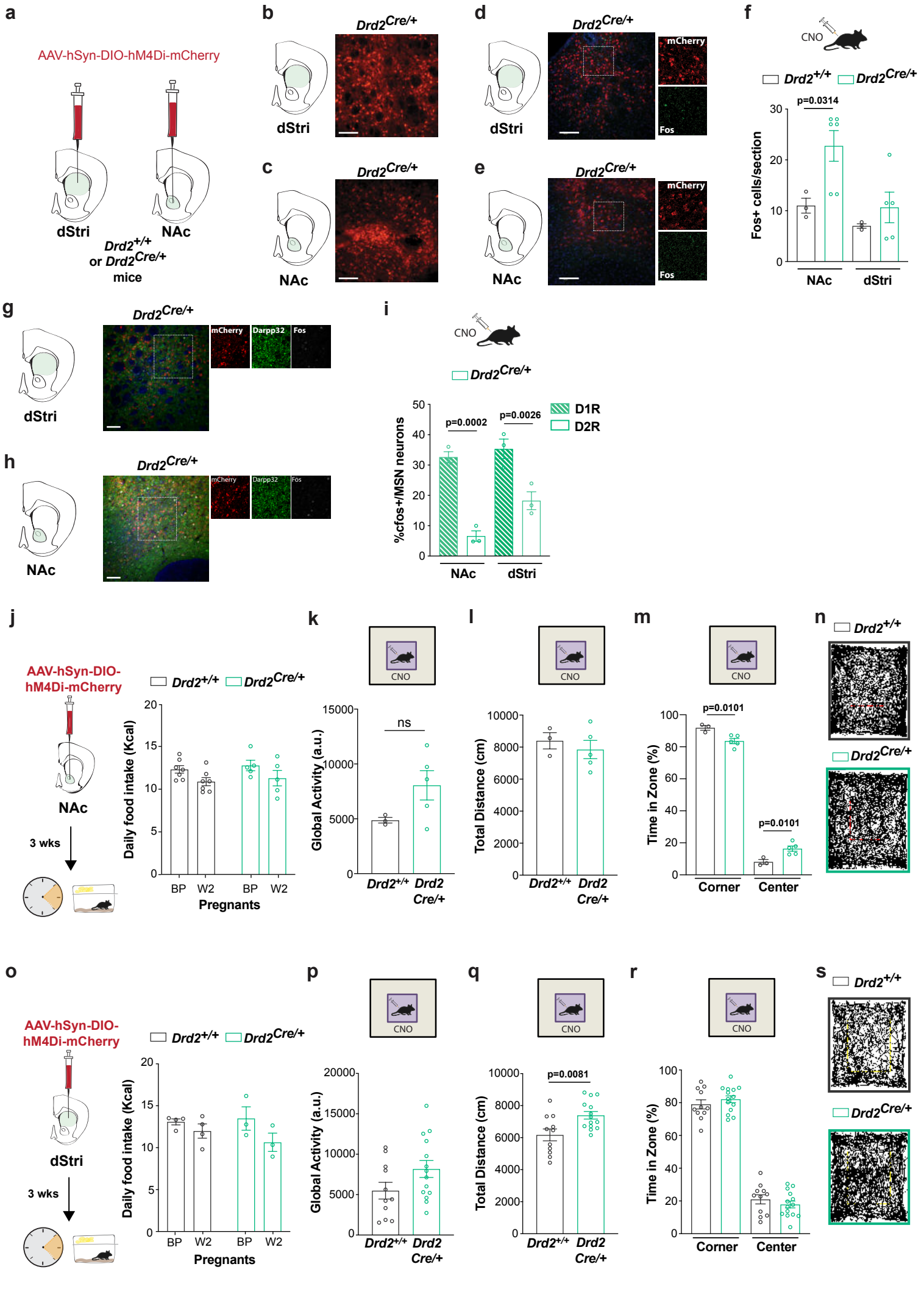

Extended Data Figure 8

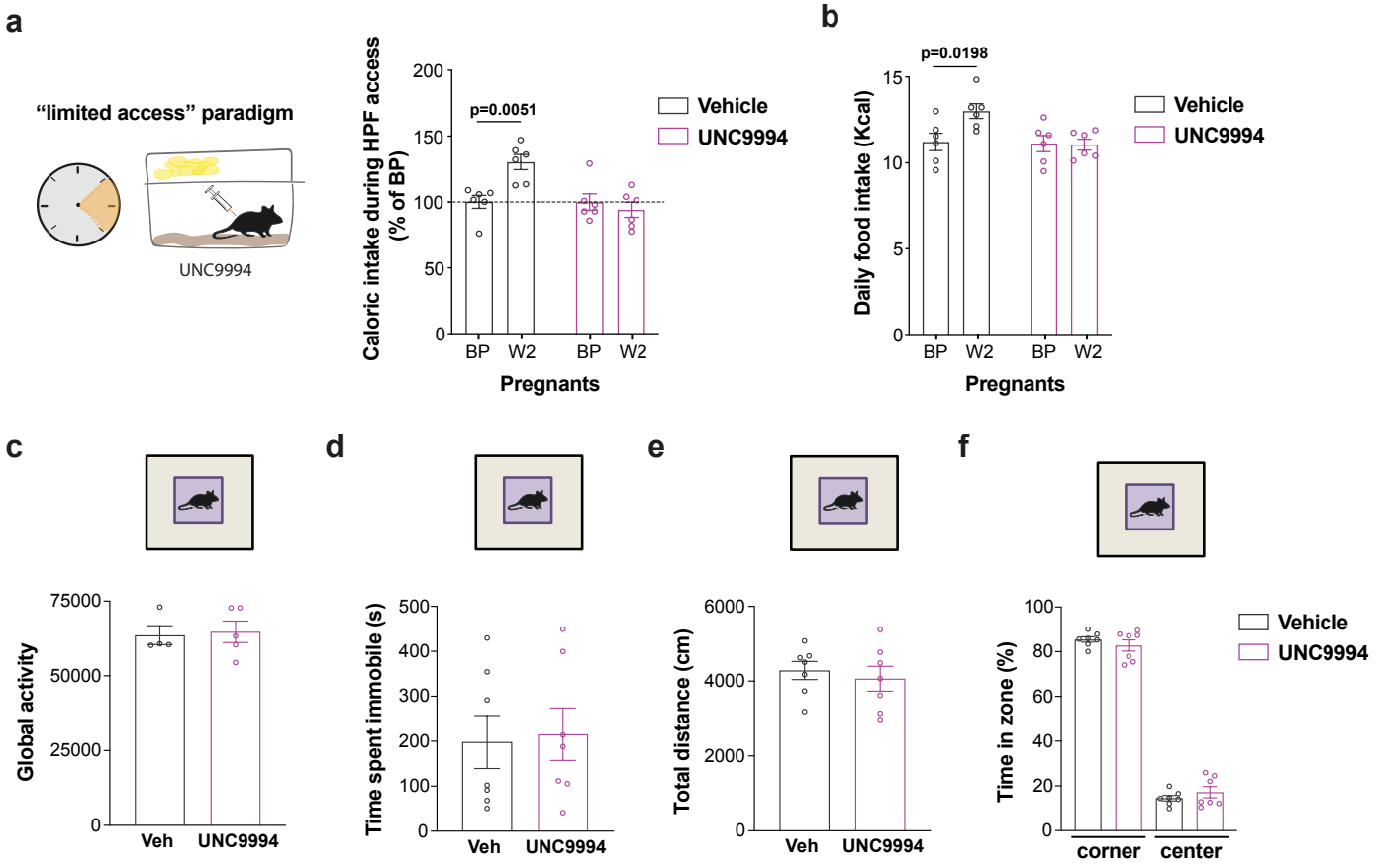

Extended Data Figure 9

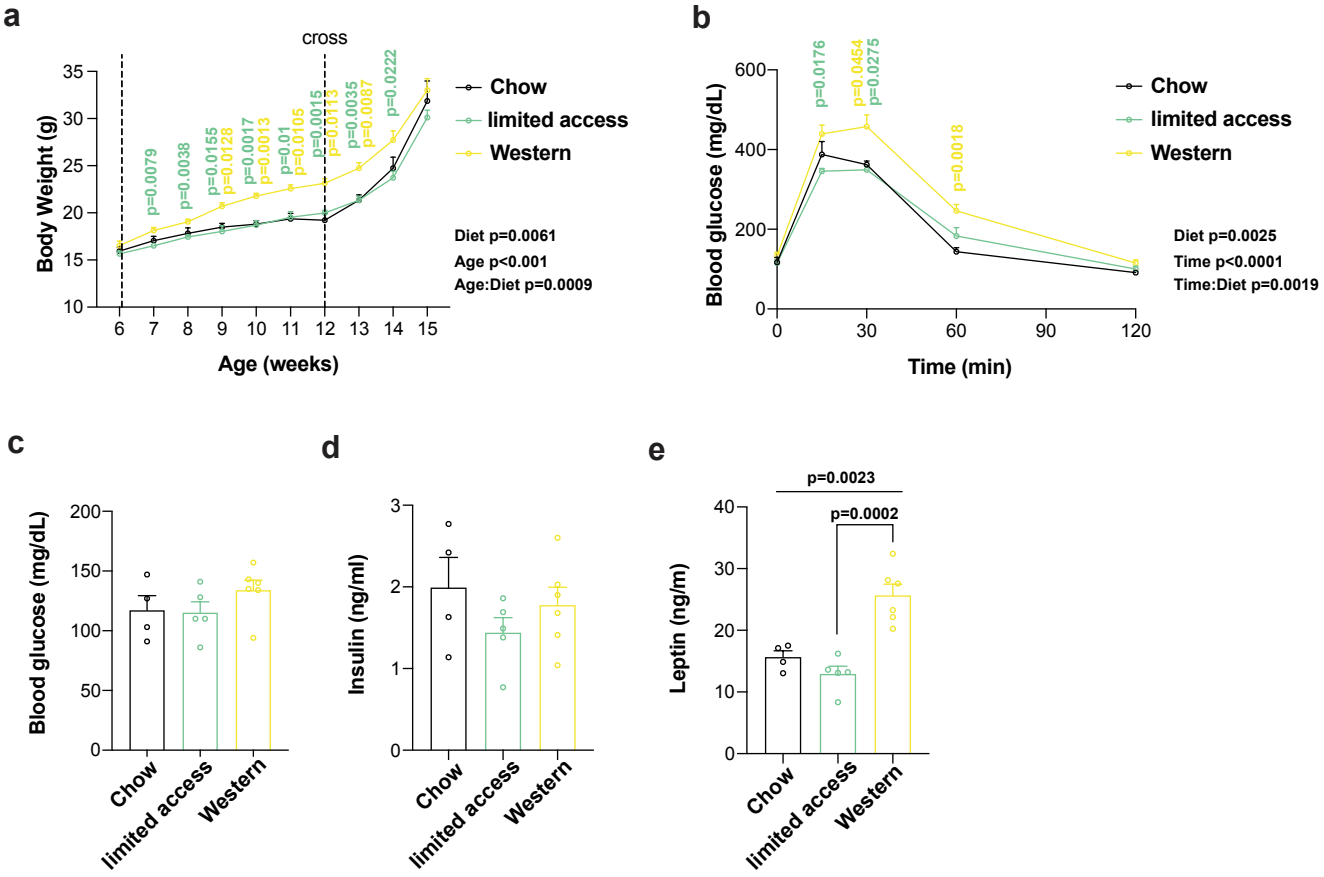

Extended Data Figure 10